Review Article

Flow Visualization in Centrifugal Pumps: A Review of Methods and Experimental Studies

Rodolfo Marcilli Perissinotto [1,*], William Monte Verde [2], Jorge Luiz Biazussi [2], Natan Augusto Vieira Bulgarelli [1], William Denner Pires Fonseca [1], Marcelo Souza de Castro [1], Erick de Moraes Franklin [1], Antonio Carlos Bannwart [1]

[1] School of Mechanical Engineering, University of Campinas, Brazil
[2] Center for Petroleum Studies, University of Campinas, Brazil
* Correspondence: rodolfomp@fem.unicamp.br

Submitted to *ELSEVIER - Journal of Petroleum Science and Engineering* on 24th July 2020.
Revised and resubmitted on 24th January 2021.

Abstract: Methods for flow visualization have been decisive for the historical development of fluid mechanics. In recent years, technological advances in cameras, lasers, and other devices improved the accuracy and reliability of methods such as *High-Speed Imaging* (HSI) and *Particle Image Velocimetry* (PIV), which have become more efficient in visualizing complex transient flows. Thus, the study of centrifugal pumps now relies on experimental techniques that enable a quantitative characterization of single- and two-phase flows within impellers and diffusers. This is particularly important for oil production, which massively employs the so-called *Electrical Submersible Pump* (ESP), whose performance depends on the behavior of bubbles and drops inside its impellers. Visualization methods are frequently used to study gas-liquid flows in pumps; however, the visualization of liquid-liquid dispersions is complex and less common, with few publications available. Methods to characterize the motion of gas bubbles are often unsuitable for liquid drops, especially when these drops are arranged as emulsions. In this context, there is room to expand the use of visualization techniques to study liquid-liquid mixtures in pumps, in order to improve the comprehension of phenomena such as effective viscosity and phase inversion with focus on the proposition of mathematical models, for example. This is a main motivation for this paper, which presents a review of researches available in the literature on flow visualization in centrifugal pumps. A broad set of studies are reported to provide the reader with a complete summary of the main practices adopted and results achieved by scientists worldwide. The paper compares the methods, investigates their advantages and limitations, and suggests future studies that may complement the knowledge and fill the current gaps on the visualization of single-phase flows, gas-liquid, and liquid-liquid mixtures.

Keywords: centrifugal pump, electrical submersible pump, flow visualization, single-phase flow, two-phase flow, high-speed imaging, particle tracking velocimetry, laser doppler velocimetry, particle image velocimetry, optical microscopy.

1. Introduction and Motivation

The design of fluid machinery is the most frequent engineering application in the field of fluid mechanics nowadays (White, 2011). In fact, pumps have been used since 1000 BC by African, Asian, Babylonian and Roman civilizations, according to historical records (Wilson, 1982). In this sense, pumps may be classified as one of the oldest known method of transferring energy to fluids in order to transport them.

In the petroleum industry, pumps are used in various stages of the production chain, especially as artificial lift methods which vertically transport the fluids stored in the reservoir, which must flow through the well, from the bottom to the surface. In this process, the pump must supply the fluids with enough energy to compensate for pressure losses caused by friction and gravity, with the aim of reaching a large flow rate at reasonable economical costs.

In fact, artificial lift methods play a key role in maintaining the oil production in mature fields, whose reservoirs usually have insufficient energy to expel the fluids properly (Al-Fatlawi et al., 2015; Al-Juboori et al., 2020). In addition, artificial lift methods are an essential strategy in heavy oil fields, where the fluid properties may impair the recovery rates (Worth et al., 2019). Thus, the development of artificial lift technologies has been crucial to increase the oil exploitation, which has consequently improved the production of derivatives necessary to meet the ever-growing global demands (Cortes et al., 2019).

One of the most common artificial lift methods that relies on centrifugal pumps is the *Electrical Submersible Pumping* (ESP system). Its main component is the *Electrical Submersible Pump* (ESP) which consists of a multi-stage pump with a sequence of impellers and diffusers. It is estimated that about 10% of the world's oil supply comes from ESP systems (Takacs, 2017) installed in more than 150,000 oil wells in operation today (Flatern, 2015). In essence, the centrifugal pumps would represent 20% of the world's electricity demand (Volk, 2013), a number which reveals the enormous relevance of pumping systems, not only for the petroleum industry, but for human activities as a whole.

The centrifugal pumps used in ESP systems are able to work at high production flow rates and high temperatures, both in onshore and offshore wells (Bremner et al., 2006). Therefore, the ESP is an efficient and flexible device, which clearly has numerous operational advantages over other artificial lift methods. However, although the centrifugal pumps are widely used in petroleum installations, several aspects related to their functioning are still problematic.

The operational issues that affect ESP systems are generally related to the characteristics of the pumped fluid. Oil production usually involves multiphase flows composed of gases, liquids, solids. Below the saturation pressure, the lighter fractions of the oil compose the gaseous phase. The heavier fractions of hydrocarbons form the viscous liquid phase, in which connate water or injected water may be also existent. Furthermore, the solid phase comes from the erosion of the reservoir rock. As centrifugal pumps are fundamentally designed to work with incompressible and low viscous fluids, the presence of a compressible phase, or water-oil mixtures that can form highly viscous emulsions, are limiting factors to their functioning. Regarding the operation with multiphase flows or viscous fluids, for example, centrifugal pumps usually experience efficiency losses in addition to instabilities that can lead to undesired consequences, such as drop in oil production, reduction in pump lifetime, and increase in well interventions. In practical terms, in a global economy that consumes 100 million barrels of oil per day (U.S. Energy Information Administration, 2020), malfunctions in ESP systems can generate significant losses to companies from the oil and gas sector.

In a scenario of insufficient oil production, with a forecast deficit of 80 to 105 million barrels per day in 2050 (Equinor, 2019), there is an evident need to seek innovation with the improvement of technologies which may enhance the efficiency of centrifugal pumps and, consequently, increase the oil supply in the coming years. In view of this necessity, the scientific community has endeavored to improve the understanding on the physical phenomena which occur in single-phase and two-phase flows within impellers and diffusers, since the characteristics of these flows strongly influence the behavior and performance of centrifugal pumps.

From the experimental investigations available in literature, it is explicit that the utilization of flow visualization methods has become more frequent over time. A quick search at Scopus database reveals an intense growth in the number of publications containing the expression *flow visualization* in their abstracts or keywords: in the 1970s the number was only 100 publications per year; in the 2000s the mark of 1000 per year was reached; and in 2019 more than 2500 documents related to flow visualization were published. The development of technologies as laser generators, digital cameras, and computers with high processing capacity has culminated in the popularization of non-intrusive optical techniques for flow visualization. The most prevalent methods are based on the tracking of tracer particles, as in the case of *Particle Tracking Velocimetry* (PTV), *Laser-Doppler Velocimetry* (LDV) and *Particle Image Velocimetry* (PIV) (Willert and Gharib, 1991; Grant, 1997; Wulff, 2006).

In the instance of single-phase flows in centrifugal pumps, it is possible to mention Wuibaut et al. (2002), Pedersen et al. (2003), Krause et al. (2006), Feng et al. (2009), Wu et al. (2009, 2011), Yang et al. (2012), Keller et al. (2014), Mittag and Gabi (2016), Gerlach (2018), in addition to Li et al. (2020), who used LDV and PIV with laser beams, high-speed cameras, and seeding tracers. The utilization of such techniques, however, require the development of transparent pump prototypes to ensure an adequate visualization inside impellers and diffusers.

Regarding the visualization of two-phase gas-liquid flows in pumps, Estevam (2002), Gamboa and Prado (2010), Trevisan and Prado (2010, 2011), Barrios and Prado (2011a, 2011b), Zhang et al. (2016), Monte Verde (2016), Monte Verde et al. (2017), Shao et al. (2018), and Zhao et al. (2021) can be cited. The authors used *High-Speed Imaging* (HSI) with high-speed cameras to identify flow patterns in rotating impellers and to evaluate the dependence of the pump performance on the gas volume fraction. Besides, a technique based on PTV was adopted by other authors, such as Perissinotto et al. (2017), Stel et al. (2019), and Cubas et al. (2020), with the objective of tracking individual bubbles to investigate their dynamics in environments subjected to intense centrifugal accelerations.

Nevertheless, it is notorious the lack of studies on the visualization of two-phase liquid-liquid flows available in the literature. Ibrahim and Maloka (2006), Khalil et al. (2006, 2008), Morales et al. (2012), Bulgarelli (2018), Schäfer et al. (2019), Bulgarelli et al. (2020a, 2020b), Valdés et al. (2020), and Schmitt et al. (2021) are examples of researchers who focused their efforts on the visualization of dispersions in centrifugal pumps. In most studies, the authors used devices such as *Laser Particle Size Analyzer* (LPSA), *Ultrasonic Extinction Spectrometer* (UES), *Optical Multimode Online Probe* (OMOP), and *Endoscope Measuring Probe* (EMP) to characterize two-phase liquid-liquid emulsions. However, the visualization of individual drops inside the impeller, with HSI and PTV methodologies, has been achieved only by Perissinotto (2018) and Perissinotto et al. (2019a, 2019b, 2020) for larger drops in water-oil dispersions.

This review article aims to examine the main experimental researches on visualization of single- and two-phase flows in centrifugal pumps available in the literature. The studies reported in this paper are important to understand the flows inside impellers and relate them to the performance of centrifugal pumps. However, as this paper will expose, there are still several aspects to be explored in future works through the use of visualization methods, such as PIV in two-phase liquid-liquid flows, for example. Besides, advancements in flow visualization may contribute for the proposition and validation of new mathematical models to predict the pressure increment generated by pumps or to represent the dynamics of liquid drops in impellers and diffusers.

This review article is divided into five sections. Section 2 discusses the major attributes of ESP systems and the problems caused by multiphase flows in centrifugal pumps. Section 3 describes the most relevant visualization methods currently available: HSI, PTV, LDV, and PIV. Then, Section 4 reviews a set of experimental studies on flow visualization in centrifugal pumps with attention to the petroleum industry. Section 5 finally brings a conclusion to the reviewed works, including the main demands from the petroleum industry, as well as suggestions for future investigations in this knowledge field.

2. Centrifugal Pumps in the Petroleum Industry

As explained in Section 1, Electrical Submersible Pumping installations are extensively used in the petroleum industry (Flatern, 2015; Takacs, 2017). A typical ESP system is essentially composed of multi-stage centrifugal pump in addition to electric motor, protector, gas separator, instrumentation, and power cable. In general, the pump consists of dozens of stages connected in series, each with an impeller and a diffuser. The impeller is a rotating component, while the diffuser is stationary, as it remains attached to the pump housing. Figure 1 displays an illustrative drawing of an ESP system configuration in an onshore well.

The operation of a centrifugal pump is related to the law of conservation of energy. Initially, the torque from the electric motor is converted into rotational motion by the pump impellers. Then, at each stage, the impeller provides kinetic energy to the fluid, while the diffuser converts part of it into pressure energy. As the stages are assembled in series, the fluid gradually gains pressure, stage after stage. Hence, the number of stages in a pump is a function of the pressure required to lift the fluids from the reservoir to the surface.

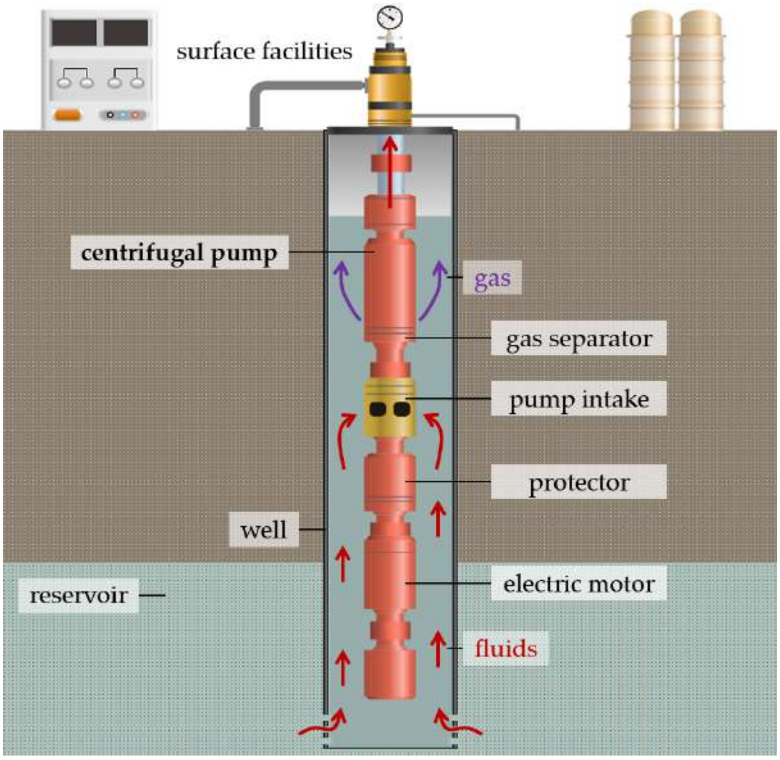

Figure 1. Typical ESP installation with downhole and surface components. A multi-stage centrifugal pump with rotative impellers and stationary diffusers is used to lift the fluids through the oil well.

2.1. Pump Performance

The amount of energy transferred by a centrifugal pump to a fluid is estimated with an energy balance at a suitable control volume. Assuming a steady state, adiabatic, and isothermal flow of an incompressible fluid, the Bernoulli head (H) calculates the energy increment generated by the pump (Fox et al., 2011):

$$H = \left(\frac{p}{\rho g} + \frac{V^2}{2g} + z\right)_{discharge} - \left(\frac{p}{\rho g} + \frac{V^2}{2g} + z\right)_{intake} \tag{1}$$

where p is the pressure in Pascal, ρ is the density of the fluid in kg/m^3, g is gravity in m/s^2, V is the average velocity of the fluid flow in m/s, and z is the vertical elevation in m, so that H symbolizes the pump head in meters of fluid column.

The velocity (V) and vertical elevation (z) may not change significantly from the pump intake to discharge. In this case, the pump head (H) is basically proportional to the pressure increment (Δp):

$$H \approx \frac{p_{discharge} - p_{intake}}{\rho g} = \frac{\Delta p}{\rho g} \tag{2}$$

The power delivered to the fluids (P_h) is traditionally named as *hydraulic power*, while the power required to drive the pump (BHP) is commonly called *brake horsepower*:

$$P_h = \rho g H Q \tag{3}$$

$$BHP = \omega T \tag{4}$$

in which Q is the volume flow rate in m^3/s, ω is the shaft angular velocity in rad/s, and T is the shaft torque in N.m, resulting a P_h and a BHP both in Watt.

Centrifugal pumps may experience hydraulic losses (e.g. viscous dissipation and disk friction), shock losses (e.g. detachment of boundary layers) and leakage losses (e.g. gaps between moving and fixed parts) that directly affect their performance (Gülich, 2008). So, the power effectively transferred to the fluid is always lower than the power consumed by the pump, as the efficiency (η) equation reveals:

$$\eta = \frac{P_h}{BHP} \tag{5}$$

Figure 2 shows the performance curves of a real pump working with a low-viscosity liquid in a single-phase flow. As can be noticed, the efficiency curve has a maximum point called *Best Efficiency Point* (BEP). It is usually recommended to operate the pumps at flow rates corresponding to BEP.

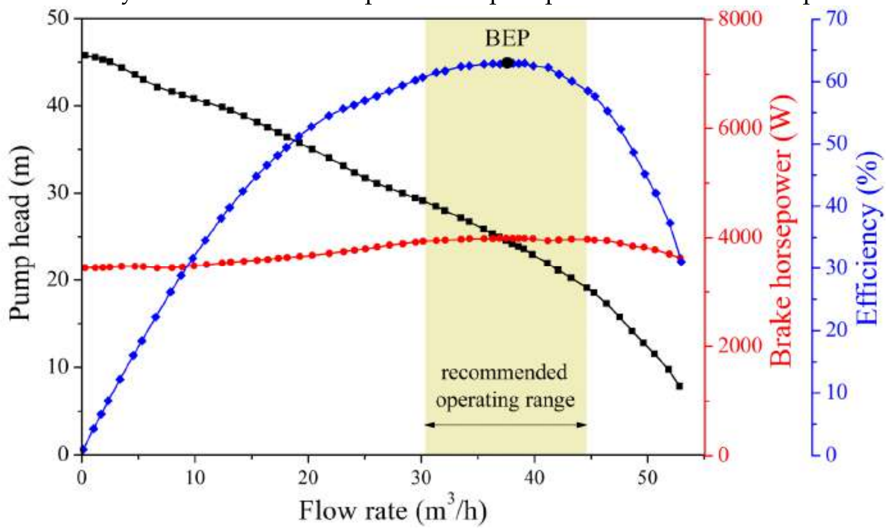

Figure 2. Performance curves for three stages of a Schlumberger GN 5200 pump working with water at 3500 revolutions per minute. The BEP is highlighted. Figure adapted from Monte Verde (2016).

The performance of centrifugal pumps is influenced by the properties of the pumped fluids and the characteristics of the flow inside the impellers. Considerable performance losses are observed in the operation with presence of gas and/or viscous liquids, a very frequent condition in applications related to the petroleum industry. The next paragraphs discuss these topics further.

2.2. Single-Phase Flow in Impellers

As illustrated in Figure 3, single-phase liquid flows in centrifugal pumps may be very complex. They are characterized by the existence of pressure and velocity fields in the impeller channels.

A congruent and well-behaved flow is generally observed when the pump operates at the flow rate that corresponds to a maximum efficiency, or BEP. However, in conditions away from the BEP, the boundary layers detach from the solid walls and consequently favor the formation of distorted velocity profiles in the impellers, with presence of jets, wakes, and recirculation zones. In this case, it is expected the occurrence of energy losses classified as *shock losses*, which are typically caused by a misalignment between the streamlines and the curvature of the blades. Besides, when the fluid has a low viscosity, the flow experiences a high turbulence which may promote the formation of vortices. The presence of vortices in an impeller influences the velocity fields and increases the energy losses due to the turbulent dissipation, classified as a type of *hydraulic losses* (Gülich, 2008).

Another important mechanism of energy dissipation is associated with the friction between the fluid flow and the solid surfaces. The energy losses due to friction, which generally increase with the square of flow rate, may depend directly either on the Reynolds number and/or on the roughness of the solid walls that compose the impeller channels. Therefore, energy losses may also occur when the centrifugal pump works with viscous fluids, a situation that causes a relevant degradation to its performance and efficiency (Gülich, 2008; Brennen, 2011). The oil production in heavy oil fields is an example of activity which demands the use of pumps in operation with single-phase viscous liquids.

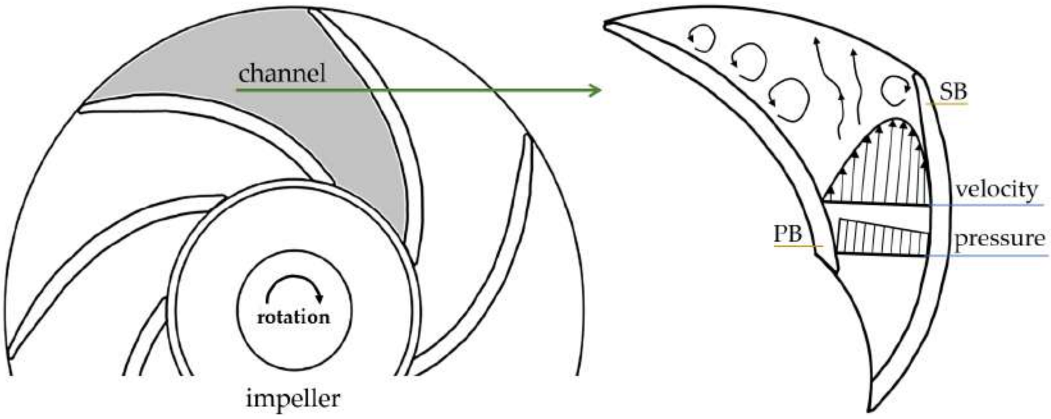

Figure 3. Illustrative drawing of pressure and velocity profiles in a single channel of an impeller that rotates clockwise. The initials PB and SB indicate the pressure blade and suction blade, respectively. The flow in impellers is characterized by the presence of jets and vortices, among other phenomena.

Visualization methods are essential to investigate single-phase flows in impellers and evaluate their influence on the performance of centrifugal pumps. In this context, it is customary to identify secondary flows and other phenomena using laser-based methods, such as *Laser Doppler Velocimetry* (LDV) and *Particle Image Velocimetry* (PIV), which are thoroughly described in Section 3. Examples of experimental studies on visualization of single-phase flows inside centrifugal pumps are discussed in detail in Section 4 as well.

2.3. Two-Phase Flow in Impellers

The occurrence of two-phase water-oil flows is frequent in oil production due to the presence of connate water originated from the pores of the sedimentary rock that composes the oil reservoir. In addition, water may occasionally come from adjacent reservoirs or even be purposely injected into the reservoir in order to stimulate the oil extraction, in a method named as water flooding (Ahmed, 2018; Rosa, 2006). In most cases, the water-oil mixture becomes arranged as an emulsion, that is, a category of dispersion that is essentially characterized by a population of small drops immersed in a continuous fluid (Sjöblom, 2005; Tadros, 2013).

When there is a high fraction of water in the oil, the two-phase water-oil dispersion may present an *effective viscosity* higher than the viscosity of the separated liquids (Guet et al., 2006; Ngan et al., 2009; Plasencia et al., 2013), a condition which generally leads to a reduction in the performance of centrifugal pumps used in ESP systems. In this regard, Bulgarelli et al. (2020a) state that dispersions and emulsions pose a great challenge for oil production, as they constitute a major issue for flow assurance, with the incidence of a phenomenon named as *phase inversion*. In a point of fact, the occurrence of operational instabilities is quite frequent in ESP systems which handle emulsions (Hartenbach et al., 2015; Honório et al., 2015), a fact that influences costs and profits of oil and gas companies.

According to Carneiro et al. (2018), the formation of emulsions depends on mechanical stirring and shearing processes that provide the energy necessary to mix the liquids and also provoke their fragmentation into small drops. In this respect, the centrifugal pumps employed in ESP systems may promote the generation of emulsions, since their rotative impellers intensely agitate the fluids. In a rotating environment, such as a pump impeller, mechanisms related to shear stress, turbulence, and interfacial instability act together to cause the rupture of one of the phases, which then acquires a morphology of dispersed drops, as exemplified in Figure 4. Over time, these drops undergo gradual breakage events so they finally assume an average size that depends on the flow conditions and also on fluid properties, such as density, viscosity, interfacial tension, and oil composition.

Figure 4. Images of water drops dispersed in mineral oil inside an impeller. As can be seen, one large drop breaks up and originates six smaller drops. Figure adapted from Perissinotto (2018).

Another condition which negatively affects the behavior of centrifugal pumps is the existence of a compressible fluid, such as natural gas, within their impellers. In fact, the incidence of two-phase gas-liquid flows is really habitual in the oil wells, where pressures can reach values lower than the liquid-vapor saturation point (bubble point), leading the lighter petroleum fractions to change their phase from a liquid to gaseous state (Shoham, 2006). Unfortunately, the presence of free gas causes a significant decrease in the performance of centrifugal pumps, with the prevalence of instabilities and reduction of pressure increment in the stages, as a consequence of phenomena known as *surging* and *gas locking* (Gülich, 2008).

Monte Verde et al. (2017) report that, when a gas is present inside an impeller, the fluid becomes arranged as a bubble. Figure 5 shows that, as the gas volume fraction increases, the slipping between gas and liquid also increases, so that the bubble grows, becomes stuck, and thus occupies a part of the useful volume of the channel. Consequently, the pressure differential generated by the pump is reduced and the energy transferred by the pump to the flow may be insufficient to transport both gas and liquid phases. In this case, the pump behaves as if it were undersized, the production rate decreases and, occasionally, it may be necessary to intervene in the oil well to resolve the problem.

As revealed by Figure 4 and Figure 5, the use of visualization methods is crucial to identify flow patterns in impellers. The shape, size, and distribution of bubbles and drops directly influence the performance of centrifugal pumps operating with two-phase gas-liquid and liquid-liquid flows. Hence, techniques as *High-Speed Imaging* (HSI) and *Particle Tracking Velocimetry* (PTV) are commonly used in order to qualitatively and quantitatively study these flows. Such methods are explained in Section 3, while some examples of experimental studies on visualization of two-phase flows within centrifugal pumps are minutely reported in Section 4.

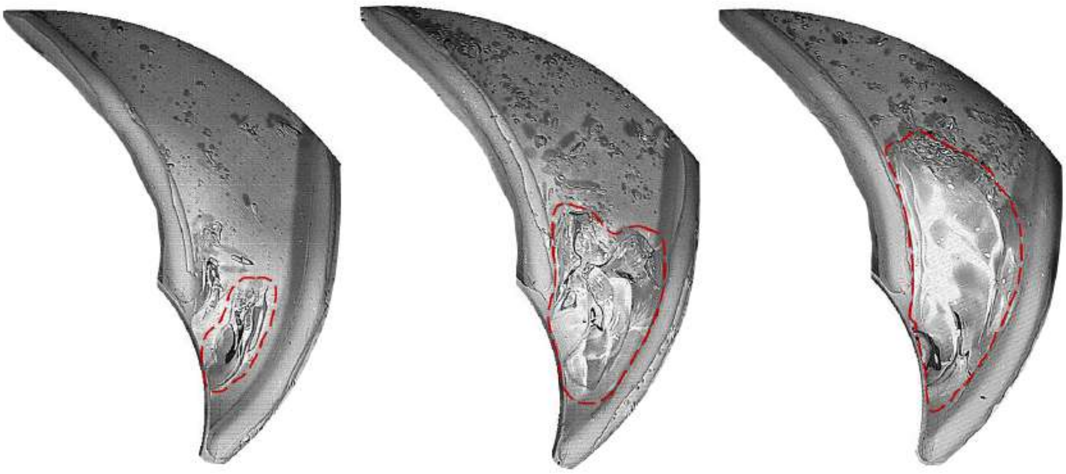

Figure 5. Images of air bubbles in water-glycerol inside an impeller. The highlighted bubble becomes larger as the gas fraction rises from 0.32% to 0.40%. Figure adapted from Monte Verde (2016).

3. Flow Visualization in Fluid Mechanics

In fluid mechanics, the analytical approaches are able to solve few problems, usually limited to laminar flows, in simple geometries, with uniform boundary conditions. In fact, most of the practical situations that involve fluid flows are physically and geometrically complex and hence demand the application of numerical or experimental approaches, such as methods for flow visualization (Fox et al., 2011).

In this context, the historical evolution of fluid mechanics has been profoundly dependent on the visualization of fluid flows. The pioneering studies are attributed to Leonardo da Vinci in about the 16th century (Lugt, 1983; Gharib et al., 2002). Ever since, many visualization experiments have been carried out, some of them by notable scientists such as Osborne Reynolds, Ludwig Prandtl, and Ernst Mach (Freymuth, 1993).

Nowadays, the methods for flow visualization are especially suitable for producing images that may be used to measure fluid velocities, identify streamlines and flow structures, estimate quantities related to turbulence, among other advantages. These techniques provide interesting qualitative and quantitative data for the study of single- and two-phase flows in engineering applications.

Flow visualization is further discussed in the following section, which describes four methods among the most relevant ones to the analysis of centrifugal pumps: *High-Speed Imaging*, *Laser Doppler Velocimetry*, *Particle Tracking Velocimetry*, and *Particle Image Velocimetry*. The methods use high-speed cameras, laser generators, and tracer particles in order to enable the observation of flow phenomena in pipelines, agitated tanks, pump impellers, among others.

3.1. Visualization with Cameras, Lasers, and Tracers

The use of tracing elements for flow visualization has become prevalent since the second half of the last century. According to Merzkirch (1987), between the 1960s and 1980s, the addition of dyes to single-phase liquid flows became a common practice that allowed the observation of streamlines, vortices, and shear layers in pipes. At the same time, the use of smokes and vapors to identify jets and wakes in single-phase gas flows, especially in wind tunnels, became usual as well. Most of these methods depended on analog cameras to capture images of the flows. Besides, they were practically limited to provide only qualitative results.

In the last twenty years, however, the advent of new technologies, such as digital cameras and laser beam generators, has engendered the development of visualization techniques that used solid seeding particles to indirectly estimate the velocity of fluid flows. This is actually the fundamental basis for the functioning of the methods (Smits and Lim, 2012) described in the next paragraphs, i.e., PTV, LDV, PIV, which often rely on HSI to work properly. Such methods are increasingly important for the study of centrifugal pumps, as they are able to provide quantitative data that improve the understanding on single- and two-phase flows within impellers and diffusers.

3.1.1. High-Speed Imaging

As discussed above, analog cameras have been used for decades to visualize single-phase flows. Essentially, these cameras were intended to work as the human eye, with the advantage of allowing the acquisition of still images of complex fluid flows. Such images used to be captured and revealed on photographic films, which limited the number of images that could be obtained and, as a result, ended up limiting the acquisition rates as well. Nevertheless, these issues have been overcome since the creation of high-speed cameras, stimulated by the development of semiconductors in addition to other technological advances in electronics and informatics (Cressler, 2016). Nowadays, high-speed cameras can work at acquisition rates in the order of hundreds of thousands of frames per second.

The high-speed camera is the main element of *High-Speed Imaging* (HSI), a visualization method that consists of shooting flows with the purpose of observing their qualitative characteristics. A lens is attached to the front of the camera to collect the light and direct it to the sensor where the image is digitally recorded. Therefore, the lens is responsible for defining the magnification of the image and ensuring the proper field of view for each experiment performed. The fundamentals on the theory of image formation are available in the practical guide by Raffel et al. (2007).

The sensors that compose the modern cameras are generally classified as *Charge Coupled Device* (CCD) and *Complementary Metal Oxide Semiconductor* (CMOS) types. In a concise manner, a sensor is basically a matrix with several individual elements, called *pixels*, which produce and store electrical charges from the absorption of incident photons of light. In the CMOS sensor, each element contains its own electronic circuit (active pixel), a characteristic that usually offers considerable advantages in comparison to the CCD sensor, including the possibility of working at high acquisition rates.

In the field of fluid mechanics, HSI has been used for several decades to identify the presence of multiphase flow patterns in pipelines and accessories (e.g. Vieira et al., 2020; Cavicchio et al., 2018; Rocha et al., 2015; Castro and Rodriguez, 2015). In addition, the technique began to be used about 20 years ago in applications related to the oil and gas sector, in order to visualize two-phase gas-liquid flow patterns. A set of studies on this subject is reviewed in Section 4.2.

As HSI has excellent temporal and spatial resolutions, the method provides the observation of fast transient phenomena and small flow structures (Mohammadi and Sharp, 2013; Thoroddsen et al., 2008) such as drops, e.g. Figure 4, and bubbles, e.g. Figure 5. However, to work properly with single-phase flows, it is recommended that high-speed cameras be used to shoot seeded flows. In fact, the addition of tracer particles to the flow is vital to ensure the estimation of quantitative data on the fluid dynamics. When HSI is used to visualize seeded flows illuminated with common light sources, a PTV method may be established, as follows.

3.1.2. Particle Tracking Velocimetry

The *Particle Tracking Velocimetry* (PTV) is a non-intrusive measurement method, based on flow visualization, which determines the velocity and trajectory of particles immersed in a moving fluid from the estimation of their displacement during a period of time. In other words, the aim of PTV is determining the fluid velocity ($\boldsymbol{U}$) from the velocity of an individual tracer ($\boldsymbol{U}_p$), which depends on its displacement ($\Delta \boldsymbol{X}_p$) and the time interval (Δt):

$$\boldsymbol{U}_p = \frac{\Delta \boldsymbol{X}_p}{\Delta t} \tag{6}$$

Both Δt and $\Delta \boldsymbol{X}_p$ are obtained from flow images captured by the high-speed camera. The former is a function of the acquisition rate, which defines the time interval between two consecutive images. The latter is measured on the images by counting the number of pixels that correspond to the tracer displacement. Thus, a calibration is necessary to convert image elements (pixels) into length units (e.g. millimeters). For a pipeline or impeller whose diameters are known, the relation between pixels and millimeters is easily established. But, if this relation is unknown, a simple way to calibrate the PTV method is to capture an image of an object such as a ruler or scale, with spatial information of physical dimensions, placed on the camera's field of view. In this case, it is possible to determine how many pixels correspond to one millimeter, for example, in the set of images captured.

In centrifugal pumps, the studies by Perissinotto et al. (2017, 2019a, 2020) are some application examples of a PTV technique. The authors tracked air bubbles, oil drops, and water drops dispersed within an impeller in order to obtain their velocities. Figure 6 illustrates the process of tracking one water drop dispersed in an oil flow. The image was acquired using a high-speed camera within the scope of HSI.

Perissinotto et al. (2017, 2019a, 2020) were interested in the study of the dispersed phases. It is important to emphasize, though, that the tracking of bubbles and drops may not correctly portray the behavior of the continuous phase. For the tracers to follow the flow rigorously, one must select particles with small diameters and also with a density similar that of the fluid, in order to minimize the differences between the velocities $\boldsymbol{U}$ and $\boldsymbol{U}_p$.

In this sense, the Stokes law estimates the velocity delay for a spherical particle with a diameter d_p and a density ρ_p immersed in a fluid with a density ρ and a viscosity μ and flowing at a constant acceleration $\boldsymbol{a}$. Although the Stokes law is valid only for low particle Reynolds numbers ($Re_p \ll 1$), it is suitable for providing reasonable results at most applications (Raffel et al., 2007):

$$\boldsymbol{U}_p - \boldsymbol{U} = d_p^2 \frac{(\rho_p - \rho)}{18\mu} \boldsymbol{a} \tag{7}$$

According to Melling (1997), seeding tracers usually have diameters in the order of units to tens of micrometers. The hollow glass microspheres are one of the most frequently used tracers, although other solid particles made of ceramic and polymeric materials are usually employed in academic and industrial applications. Aluminum oxide, titanium dioxide, and melamine resin are some examples.

(**a**) Image acquisition: HSI

(**b**) Image processing: PTV

Figure 6. Example of (a) HSI applied to visualize two-phase flows in a pump impeller and (b) PTV applied to track a single water drop in the images. The drop path is shown in red color. The position ($\boldsymbol{X}_p$) and velocity ($\boldsymbol{U}_p$) vectors at a random instant of time are represented by green and blue arrows. The figure was adapted from Perissinotto (2018).

In the PTV technique, the concentration of tracers is low enough for a particle to be individually tracked in the flow images (Dracos, 1996; Maas et al., 1993; Malik et al., 1993) with a Lagrangian approach. Hence, a large population of single particles must be tracked to ensure statistically valid results, a condition that may increase the time required for processing the images. It may be thus convenient to adopt a Eulerian procedure in which groups of particles are followed in a specific volume of fluid. This possibility may be achieved when the flow is illuminated by lasers, as in LDV and PIV methods, both described below.

3.1.3. Laser Doppler Velocimetry

When a laser beam is oriented toward a flow, it directly illuminates the moving tracers as well. The laser light is thus scattered by each particle, so that the frequency of the reflected wave changes proportionally with the tracer velocity (Nagabhushana and Sathyanarayana, 2010). Actually, this phenomenon is the basis for *Laser Doppler Velocimetry* (LDV), which consists of illuminating a fluid with two laser beams of a known wavelength (λ) and angle of inclination (θ) in order to measure, using photodetectors, the variations in the frequency of the reflected light (Δf). As a result, the local velocity of the fluid ($\boldsymbol{U}$) can be estimated (Boutier, 2013):

$$\boldsymbol{U} = \frac{\lambda \Delta f}{2\sin(\theta/2)} \tag{8}$$

Pedersen et al. (2003) and Feng et al. (2009) are examples of authors who used LDV in the last years to investigate single-phase water flows inside centrifugal pumps. A review of these studies is available in Section 4.1. In fact, LDV has been employed for decades to study external and internal flows, e.g. in wind tunnels, agitated tanks, microchannels, pipelines and accessories (Schmetterer and Garhofer, 2007; Paone et al., 2009; Molki et al., 2013). In most applications, the technique has proven to provide satisfactory measurements with acceptable uncertainties.

Although LDV is efficient in estimating quantities related to velocity, vorticity, and turbulence, it has an important limitation: the laser beam is focused on small regions of the fluid flow. A direct consequence is that, to cover large volumes, the method demands a higher computational effort with longer run times. The best alternative, in this case, is illuminating a volume of fluid with a laser sheet and then tracking a large population of particles at once. This is exactly the idea of PIV, a technique explained in the following paragraphs.

3.1.4. Particle Image Velocimetry

In the *Particle Image Velocimetry* (PIV), the tracer particles are illuminated externally by a laser sheet normally produced by a pulsed laser generator. A digital camera is placed perpendicularly to this laser sheet to record the position of a group of particles ($\boldsymbol{X}$) in consecutive instants of time (t). Then, for a known time interval (Δt), algorithms determine the displacement of these particles ($\Delta\boldsymbol{X}$) and, consequently, provide a vector that represents the local fluid velocity ($\boldsymbol{U}$):

$$\boldsymbol{U} = \frac{\Delta \boldsymbol{X}(\boldsymbol{X}, t)}{\Delta t} \tag{9}$$

The similarity between PIV and PTV is noticeable. However, the key difference between them is related to the number of tracers recorded in the flow images and the algorithm for computing the flow velocities. On the one hand, when the number of particles is low, it is possible to monitor their individual movement, so the PTV stands. On the other hand, when the number of particles is high, it is very difficult to identify their individual movement and, as a result, one must measure the average displacement of groups of tracers using statistical methods. In this case, a PIV approach is arranged.

The execution of an experiment with a two-dimensional PIV method is exemplified in Figure 7, in which it is possible to observe the main components of a typical system: a laser generator, a digital camera, as well as an electronic circuit responsible for synchronizing each pulse emitted by the laser with each image captured by the camera. In addition, a set of mirrors and lenses is fixed in front of the laser cavity to convert the light beam into a thin sheet that finally illuminates a plane region of the flow.

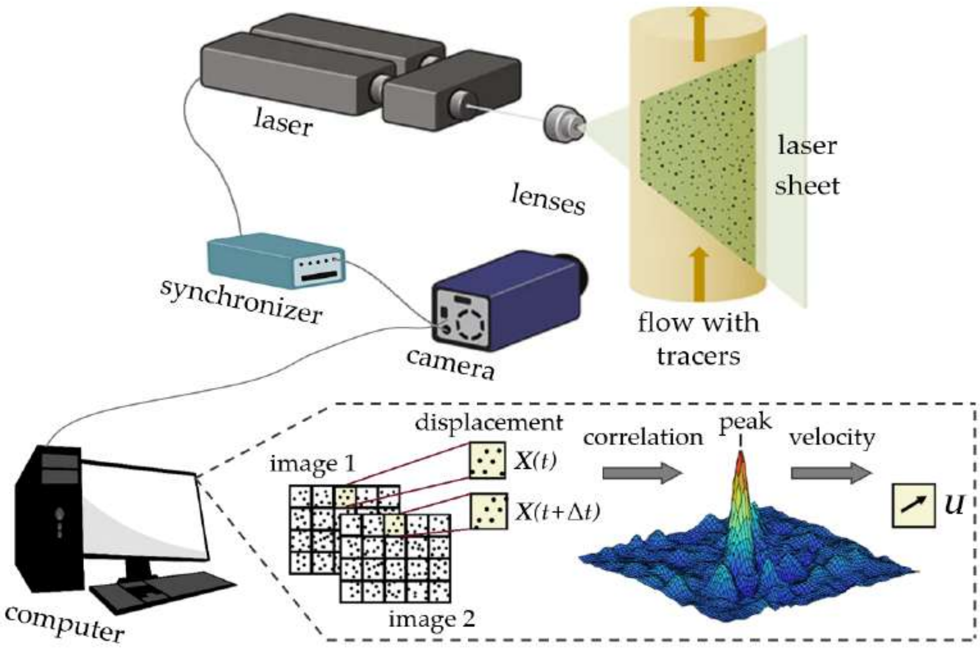

Figure 7. Illustrative scheme of a conventional PIV system (2D-2C PIV) used in a generic experiment. The dashed lines highlight the image processing with a cross correlation routine which calculates the displacement of tracer particles ($\boldsymbol{X}$) to estimate the local fluid velocity ($\boldsymbol{U}$).

All the devices must be connected to a computer that processes the images to calculate the fluid velocity vectors and other quantities dependent on their derivatives and integrals, such as gradient tensors, vorticity vectors, linear and angular deformations, streamlines, and circulation integrals that reveal the presence of vortices (Adrian and Westerweel, 2011). The procedure basically consists in dividing each pair of images into small regions, called interrogation windows, and then identifying the movement of the particles from differences in light intensity. The statistical concept of correlation is then used to calculate the average displacement of a group of tracers. In practice, the correlation is obtained with a *Fast Fourier Transform* (FFT) which reduces the computational effort (Bracewell, 1999; Jähne, 2005). As a result, the algorithm provides a correlation map with a peak intensity for each pair of interrogation windows. This peak intensity corresponds to a velocity vector that represents an estimated measure of the local fluid velocity. The algorithm is then repeated for other interrogation windows and other pairs of flow images as well. Detailed information on image processing practices is provided by Raffel et al. (2007).

In conventional PIV, as can be seen in Figure 7, a single camera is placed perpendicularly to the laser sheet. In that configuration, the method measures two components of the velocity vector in a two-dimensional region (2D-2C PIV). However, in more complex flows, the combination of two or more cameras is recommended to estimate all three components of the velocity vector. In this case, the method is called *stereoscopic* PIV, or simply *stereo*-PIV (2D-3C), when the measurements are done on a thin laser plane and *tomographic* PIV, or simply *tomo*-PIV (3D-3C), when the measurements are done within a thick laser volume. Figure 8 illustrates these variations of the PIV technique.

According to Raffel et al. (2007), the calibration of a 2D-2C PIV setup relies on images of targets which must be placed coincident with the light sheet plane. The targets typically consist of precise grids of markers, as dots, crosses, or lines, easily detected with simple image processing techniques. A single image is thus sufficient to determine a linear enlargement factor between the image space and the object space. However, any misalignment between calibration plane and illuminated plane leads to rather large errors that require a correction based on the vector field (Scarano et al., 2005).

In the case of 2D-3C PIV, the optical arrangement introduces a strong distortion effect, so that the magnification factor is no longer linear. The calibration procedure usually consists in taking several images of a flat calibration grid, placed initially in the laser plane, and afterward in a few other parallel planes (Brossard et al., 2009). Calibration data can be improved with a self-calibration method, which detects and corrects small discrepancies between de-warped images recorded by the two cameras at the same time. In addition, new techniques have recently been developed, such as calibration based on pinhole models, an approach capable of accurately recovering the out-of-plane velocity with mapping functions derived from perspective equations (Wieneke, 2005; Giordano and Astarita, 2009; Van Houwelingen et al., 2020).

In the 3D-3C PIV, the calibration procedure does not map the position of a specific illuminated plane, but extends over a finite interval of the physical space. As a positive consequence, it does not require any alignment between calibration target and illuminated plane. However, the requirements on calibration errors for tomo-PIV are considerably stricter than those for stereo-PIV. They involve some factors such as mechanical instabilities on the camera supports, clearance in the lens adapters, and vibrations and temperature variations inside the cameras (Scarano, 2012; Schosser et al., 2016).

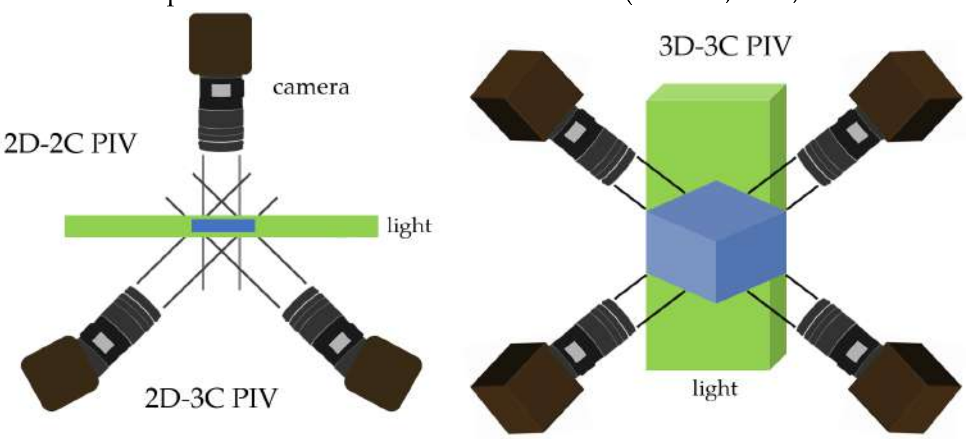

Figure 8. Typical positions of cameras in conventional (2D-2C PIV), stereographic (2D-3C PIV), and tomographic (3D-3C PIV) systems with one, two, and four devices, respectively.

Laser light is basically a monochromatic, coherent and directional electromagnetic radiation (Renk, 2017). The laser used in PIV has a high energy density and a precise pulse control, attributes that reinforce its advantages over ordinary light. Most solid-state laser sources used in PIV systems are classified as Nd:YAG, an acronym that indicates that light is emitted by the crystal $Nd{:}Y_3Al_5O_{12}$, consisting of neodymium ions incorporated in an yttrium-aluminum garnet. The radiation from a Nd:YAG crystal is infrared but an electronic circuit multiplies the wave frequency to form a visible green light with a wavelength of λ = 532 nm (Raffel et al., 2007).

Laser generators used in PIV release their light in the shape of pairs of pulses. Each individual pulse lasts in the order of nano to microseconds, while the interval between two pulses that compose a single pair generally ranges from micro to milliseconds. The time interval between two consecutive pairs of pulses may reach hundreds of milliseconds, a number defined by the pulsation frequency of the laser device. Most PIV applications in fluid mechanics use lasers with low pulsation frequencies of about units to tens of Hertz in order to estimate average flow parameters. However, the study of complex flows requires the analysis of fast transient phenomena and, in this case, it is recommended to employ lasers with a higher pulse rate, sometimes above 1000 Hertz. Such lasers compose a PIV method named *time-resolved* (TR-PIV). The time intervals explained above are indicated in Figure 9, which illustrates a common type of synchronization between both the light pulsation and the image acquisition.

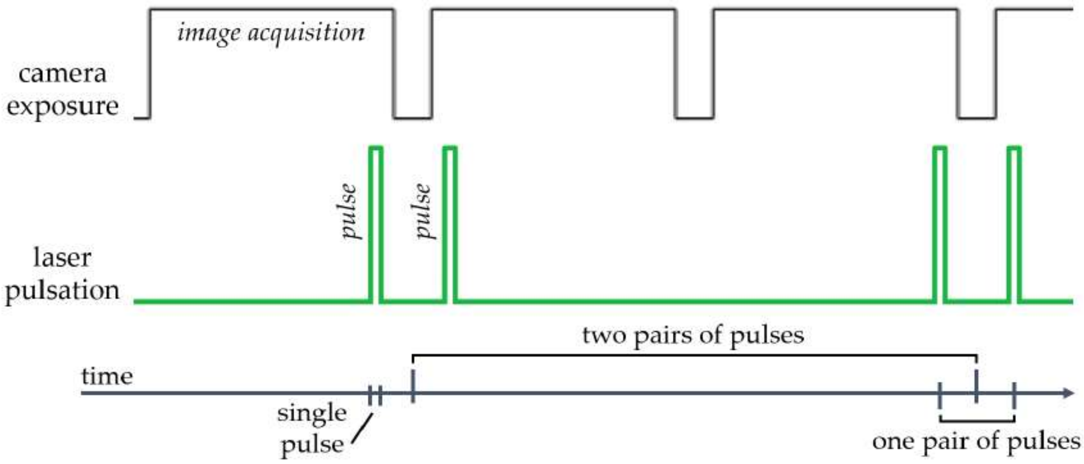

Figure 9. Frame straddling technique to synchronize the camera exposure with the laser pulsation. The durations of a single pulse, a pair, and two pairs of pulses are illustrated in a timeline.

As laser light is a type of electromagnetic radiation, it is scattered by diffraction, refraction, and reflection mechanisms when it passes through solid walls and illuminates particles in a flow. When the particle diameter (d_p) is larger than the laser wavelength (λ), Mie theory predicts that scattering is a function of several factors, such as refractive indexes of both fluid and tracers, size and shape of the particles, observation angles, among others (Abrantes et al., 2012). Figure 10 contains two examples of Mie diagrams formed by concentric circles that reveal the polar distribution of the intensity of the light scattered by two particles when receiving an incident laser light.

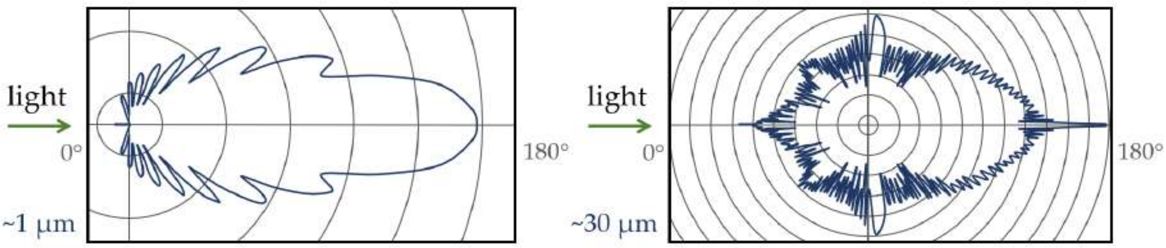

Figure 10. Typical scattering diagrams for solid particles made of borosilicate glass with diameter (d_p) of approximately 1 µm and 30 µm illuminated by light with wavelength (λ) of about 532 nm.

In single-phase flows, polished solid surfaces and metallic objects in the test section excessively reflect the laser light, which may saturate and damage the camera sensor. In parallel, in multiphase flows, gas-liquid interfaces represent a source of reflections that may affect the image quality while dispersed bubbles and drops may complicate the identification of tracer particles. In these situations, a *laser-induced fluorescence* (LIF-PIV) strategy is recommended to reduce undesired reflections, ensure durability for the camera, and improve the distinction between tracers and other solids occasionally found in the flow, as fragments of dirt, sand, pollen, among others (Raffel et al., 2007). The LIF-PIV essentially consists of adding fluorescent particles to the flow and installing optical filters in front of the camera lens. With the Nd:YAG laser, it is customary to use polymeric microspheres doped with rhodamine, a dye that absorbs the incident green light and emits other wavelengths with reddish tones (Abrantes et al., 2012).

The refraction phenomenon, otherwise, distorts the laser sheet and may consequently promote an increment in measurement uncertainties. A habitual manner of mitigating undesired refractions is through the selection of fluid and solid materials with identical refractive indexes. This strategy is named as *refractive index matching* (RIM-PIV). The RIM-PIV practice frequently uses glycerol, mineral oil, or mixtures of water and sodium iodide to study flows in pipes and vessels made of transparent polymers such as acrylic glass (Budwig, 1994). In this case, both the fluid and solid have a refractive index of about 1.50, so that the laser sheet traverses them with minimal distortion.

The main variations of the PIV method, as presented in this section, are summarized in Table 1.

Table 1. Summary of PIV procedures currently employed in flow visualization studies.

Method	Characteristics	Advantages
2D-2C PIV	Conventional planar PIV with one digital camera.	Average velocity vectors (and derived quantities) with two components in two dimensions.
2D-3C PIV 3D-3C PIV	Stereographic and tomographic PIV with two or more cameras.	Average velocity vectors (and derived quantities) with three components in two or three dimensions.
TR-PIV	Laser generator with a high pulsating frequency.	Instantaneous velocity vectors and fluctuations. Detection of fast transient phenomena.
LIF-PIV	Fluorescent seeding tracers and optical bandpass filters.	Reduction of light reflection to protect camera sensor and yield better results.
RIM-PIV	Fluid and solid walls with the same refractive index.	Reduction of light refraction to control the correct shape of the laser sheet.

The PIV method has been used since the 1980s to study flows in pipelines and their accessories (Buchhave, 1992; Adrian, 2005). This popular and powerful method is often successful in providing reliable and detailed data on the behavior of complex flows (Willert and Gharib, 1991; Grant, 1997; Wulff, 2006). In the regard of centrifugal pumps, many researchers used 2D-2C PIV or 2D-3C PIV, sometimes together with TR-PIV (e.g. Krause et al., 2006; Mittag and Gabi, 2016), or LIF-PIV (e.g. Pedersen et al., 2003; Krause et al., 2006; Wu et al., 2009; Keller et al., 2014), or RIM-PIV (e.g. Wu et al., 2011; Mittag and Gabi, 2016), to investigate single-phase flows in impellers and volutes. A review of these studies is performed in Section 4.1 below.

4. Experimental Studies

The first formal studies on single-phase flow in centrifugal pumps started to be published at the beginning of the last century. In this vein, books by Stepanoff (1957) and Pfleiderer and Petermann (1979) have brought together a wide range of concepts and theories. Although they were elaborated more than half a century ago, these books have retained an appreciable relevance for the analysis of turbomachinery until today.

Developed more recently, the book by Gülich (2008) is a reference for single- and two-phase flows in pump impellers, a subject discussed in Section 2 of this review article. The book deals with viscous flows and their consequences for pump performance, a high-priority issue for the Electrical Submersible Pumping systems employed in the petroleum industry to lift heavy oils and water-oil emulsions. Methods for correcting the performance of such pumps working with viscous fluids are available in the ANSI-HI 9.6.7 standard (2010) and in the study by Monte Verde (2016).

Over the last twenty years, the knowledge of engineers and researchers with regard to single- and two-phase flows in centrifugal pumps has advanced considerably. In practice, the development of visualization methods, such as *High-Speed Imaging* and *Particle Image Velocimetry* presented above in Section 3, has conducted science to a greater understanding on the phenomena that delineate the flows in impellers, usually marked by the presence of velocity profiles, secondary flows, as well as gas bubbles and liquid drops.

From this background, Section 4.1 and Section 4.2 are dedicated to reviewing a set of important studies available in literature on the visualization of single- and two-phase flows within fixed and moving parts of centrifugal pumps.

4.1. Single-Phase Flows in Centrifugal Pumps

The study by Wernet (2000) reports the first visualization experiments in turbomachines after the development of digital methods related to PIV. According to the author, Paone et al. (1989) were the pioneers to use PIV to investigate a single-phase flow in a centrifugal pump, with focus on its volute diffuser. The research was extended by Dong et al. (1992a, 1992b), who estimated momentum and energy fluxes, turbulent stresses, and turbulence production in a pump volute, then measured velocity fluctuations near an impeller exit, and also identified pulsating structures in the fluid flow. All these experiments were performed at a time when the digital cameras were still an incipient technology, in a situation that induced the researchers to use analog cameras whose images had to be captured and revealed on photographic films made from silver salt crystals.

Akin and Rockwell (1994) and Sinha and Katz (2000) are among the first ones to use the PIV to investigate the flow in the gap between a pump impeller and diffuser. The authors identified the formation of turbulent structures, such as jets and wakes, depending on the geometric orientation of the impeller blades. According to them, the rotating impeller of a centrifugal pump may promote the occurrence of hydrodynamic instabilities which affect the structure of the boundary layers in the blade walls, occasionally causing the separation of the flow within the adjacent diffuser.

Over time, PIV methods have become increasingly accessible and efficient, due to the improved processing capacity of computers and the popularization of digital cameras. Hence, since the 2000s, there has been an increase in the number of publications on single-phase flows in centrifugal pump impellers analyzed with PIV. The next paragraphs describe the most recent advances related to this subject, with studies by Wuibaut et al. (2002), Pedersen et al. (2003), Krause et al. (2006), Feng et al. (2009), Wu et al. (2009, 2011), Yang et al. (2012), Keller et al. (2014), Mittag and Gabi (2016), Gerlach (2018), in addition to Li et al. (2020).

Wuibaut et al. (2002) analyzed a radial flow pump working with single-phase air flow, in which polyethylene glycol particles were added as tracers. Experiments were conducted at a rotation speed of 1710 revolutions per minute (rpm), at six air flow rates from 26% to 161% of the design condition, also named as *Best Efficiency Point*. Two regions next to the impeller outlet and the vaneless diffuser inlet were illuminated by a Nd:YAG laser light, as a part of a traditional 2D-2C PIV. As main results, the researchers obtained charts with average velocities and observed the formation of wakes and jets related to air velocity fluctuations. In addition, at the lowest flow rates, intense instabilities arose in the diffuser and then spread to the impeller, leading to the prevalence of unsteady flow patterns. The authors claimed that the most relevant limitation of their methodology was precisely associated with the results for the off-design flow rates possibly by reason of an insufficient temporal resolution.

Pedersen et al. (2003) carried out experiments using both *Laser Doppler Velocimetry* and *Particle Image Velocimetry* methods in one of the impellers of a two-stage transparent pump prototype. The authors investigated the water flow at a rotational speed of 725 rpm for flow rates between 25% and 100% of the BEP. The time interval between two single laser shots was adjusted to a corresponding rotation angle of 0.6 degree (or 0.01 rad), while each pair of laser shots was triggered after every 15 complete impeller revolutions. Therefore, the authors obtained velocity curves and turbulent kinetic energy maps as results. Figure 11 reveals that, for the design flow rate, the flow remained congruent and well-behaved; however, at a lower flow rate, an irregular velocity profile was arranged with the consequent separation of the impeller channels into two parts, a condition that caused the formation of recirculation cells and nonrotating stalls.

In a general way, according to Pedersen et al. (2003), such results achieved with LDV and PIV are quite similar, but the PIV method presents two advantages over LDV, which are a considerably reduced run time and an additional ability to identify instantaneous spatial flow structures. Hence, the authors concluded that the PIV technique is generally efficient in providing reliable and detailed velocity data inside full impeller channels, especially when fluorescent particles are used as tracers. More information on experiments and results can be found in the PhD thesis by Pedersen (2000).

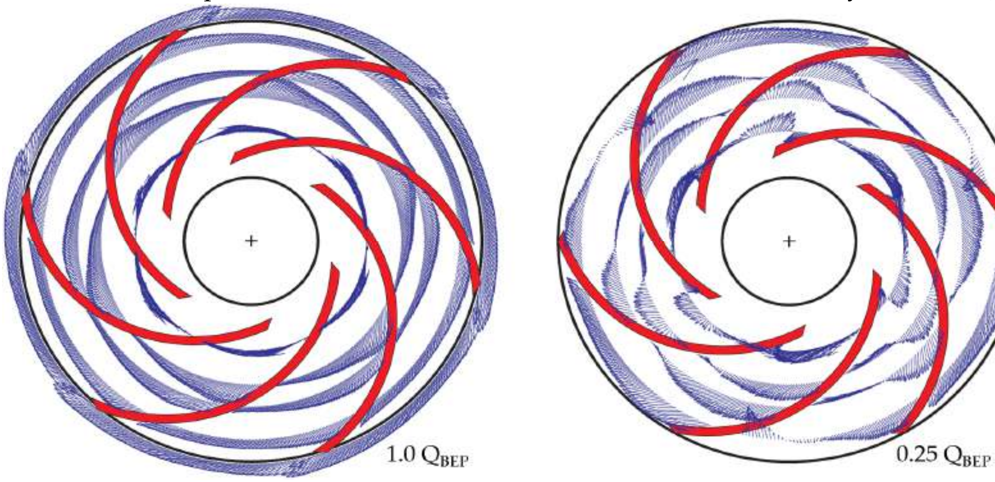

Figure 11. Vector plot of relative velocity measured in an impeller with LDV at five radial positions. As can be observed, the characteristics of the velocity profile sharply depend on the water flow rate. Figure adapted from Pedersen (2000).

A comparative investigation between LDV and PIV was also executed by Feng et al. (2009), who used a Nd:YAG laser as illumination source and polyamide particles as flow tracers. The researchers studied a water flow in the impeller channel of a transparent pump prototype working at 1450 rpm. The results include velocity fields and turbulent kinetic energy maps, both in the region between the impeller outlet and the diffuser inlet, as displayed in Figure 12 and Figure 13. A jet-wake structure was detected in the same region, with a high velocity and a low turbulence on the pressure side, but with a low velocity and an intense turbulence on the suction side of the blades. When comparing the experimental data, the authors concluded that turbulence was better determined with LDV, as the measurements with PIV were often influenced by light reflections from solid surfaces.

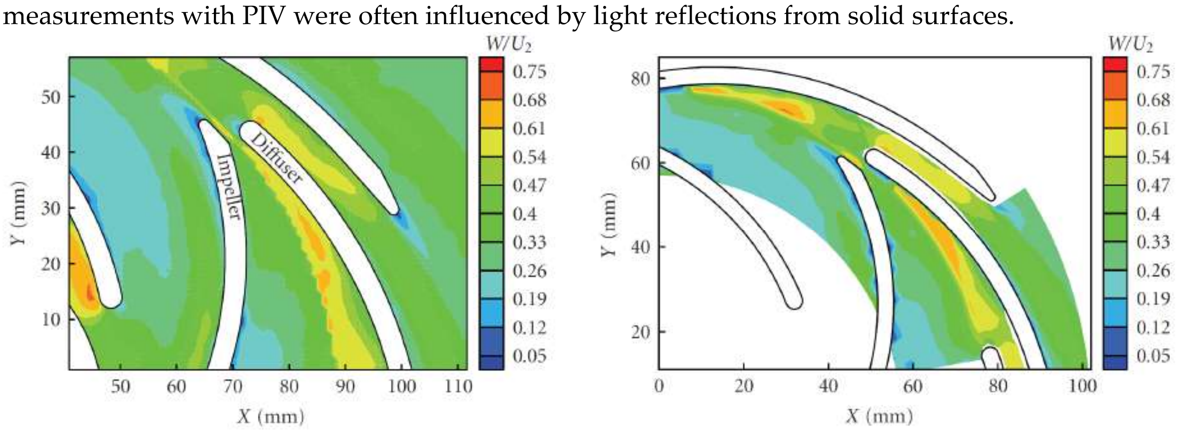

(**a**) PIV (**b**) LDV

Figure 12. Contours of relative velocity, *W*, measured with PIV and LDV at the positions *X* and *Y*. The impeller blades rotate clockwise with a velocity U_2. Figure extracted from Feng et al. (2009).

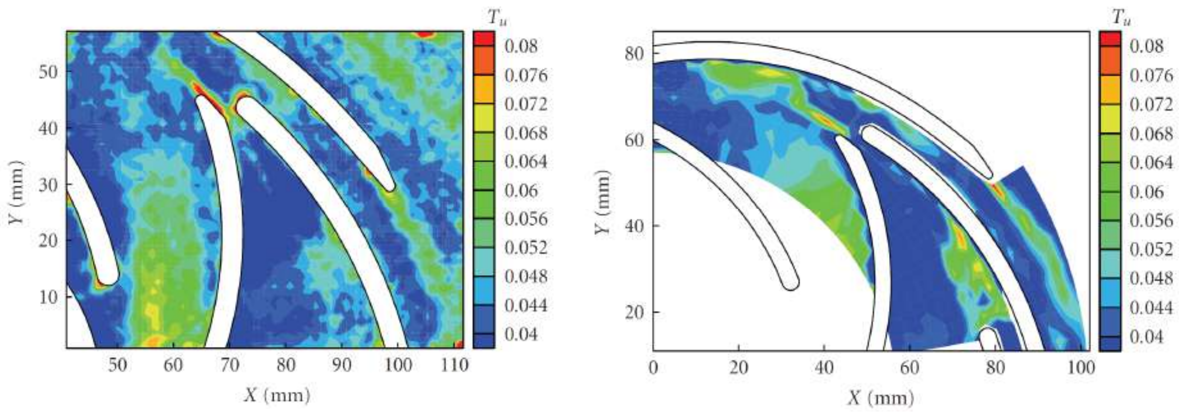

(**a**) PIV (**b**) LDV

Figure 13. Contours of turbulence intensity, *Tu*, measured with PIV and LDV at positions *X* and *Y*. *Tu* is a function of the kinetic energy and impeller velocity. Figure extracted from Feng et al. (2009).

To complete their study, Feng et al. (2009) made numerical simulations using a *Computational Fluid Dynamics* (CFD) methodology. Despite the satisfactory results, the authors concluded that the numerical simulations underestimated the turbulence rates, in comparison with the data measured with PIV. Similarly, other authors such as Byskov et al. (2003), Cavazzini et al. (2009), and Westra et al. (2010) also compared experimental with numerical results and observed satisfactory agreements between the different methods.

As stated by Wuibaut et al. (2002), Pedersen et al. (2003), and Feng et al. (2009), the limitations of the conventional 2D-2C PIV technique include the occurrence of light reflections from solid surfaces and the possible incapacity of detecting fast velocity fluctuations and related phenomena. These two disadvantages were partially eased by Krause et al. (2006), who used a *time-resolved* (TR-PIV) system with a high-frequency pulsed laser to investigate the existence of stall cells in a pump impeller. The authors also adopted a *laser-induced fluorescence* (LIF-PIV) procedure with tracers made of melamine resin with rhodamine dye. As discussed in Section 3, the LIF-PIV has the main objective of avoiding the light reflection to the camera lens and consequently protecting the integrity of the camera sensor.

Thus, by setting acquisition frequency rates of up to 800 Hz, Krause et al. (2006) characterized the evolution of a time-dependent flow field. The authors obtained velocities and streamlines which revealed the formation and propagation of vortices in a radial impeller. The pump rotation was set to 600 rpm while the water flow rate was set to 11.8 m^3/h, a number that corresponds to 25% of BEP. As Figure 14 shows, these two intense vortices occupied a large region of the channel passages, a condition that may explain the performance degradation typically observed when a pump operates at flow rates different from the design point.

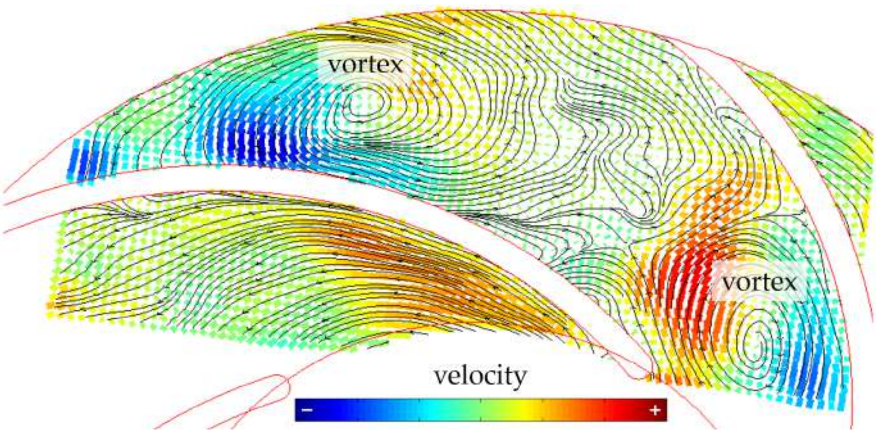

Figure 14. Blockage of an impeller channel by two strong vortices detected with TR-PIV and LIF-PIV techniques. Condition observed at 600 rpm and 25% of BEP. Figure adapted from Krause et al. (2006).

In this regard, Gerlach (2018) provided a broad study on the performance of a centrifugal pump as a function of its impeller characteristics. The author varied parameters as height and diameter of the impeller, curvature and exit angle of the blades, number of channels, and presence or absence of winglets to reduce drag. The flow analysis was performed with a conventional 2D-2C PIV in order to evaluate velocities and vorticity fields. The researcher noticed clear differences in the results and concluded that the impeller design influences the fluid behavior and, consequently, sharply impacts the pump performance – which may increase or decrease depending on the situation.

Likewise, Keller et al. (2014) executed an extensive investigation on single-phase flow in pump. The authors studied a water flow in an impeller with six channels rotating at 625 rpm. As Figure 15 shows, the authors used a common 2D-2C PIV system, with a camera and a Nd:YAG laser source, in addition to a pump prototype with transparent parts made of acrylic glass and polycarbonate. The prototype allowed visual access to two regions of interest next to the gap between the impeller and volute. Detailed information on the design and construction of this pump prototype is available in the PhD thesis by Keller (2014).

Keller et al. (2014) chose hollow glass microspheres and fluorescent particles as seeding tracers. According to the authors, the LIF-PIV has the advantage of providing reliable velocity fields even in regions close to solid boundaries, as the technique avoids reflections and reduces background noise. Among several results obtained, there are the local average velocity; the vorticity, determined from velocity derivatives; the turbulent kinetic energy, estimated from velocity variations; the turbulent kinetic energy production rate, calculated by means of the stress tensor, which depends on velocity derivatives; as well as temporal signals and frequency spectra. Thus, the authors could successfully investigate fluid-dynamic flow structures between the impeller outlet and the volute tongue.

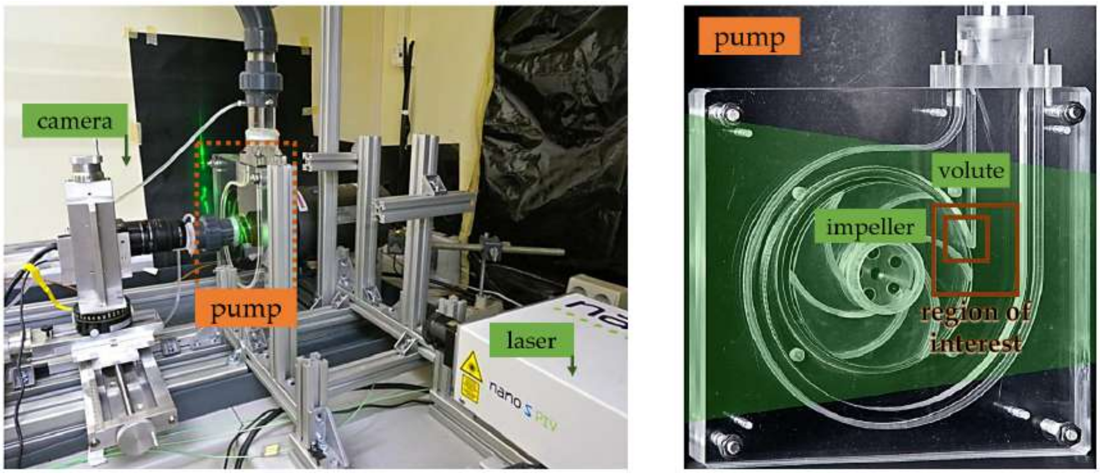

Figure 15. Facility used to perform 2D-2C PIV experiments. Figure adapted from Keller (2014).

For the flow rate corresponding to BEP, an intense positive vorticity sheet was identified in the impeller suction blade as a consequence of velocity gradients. In addition, a negative vorticity sheet was detected in the blade trailing edge. Figure 16 illustrates that, as the impeller rotates, the negative vorticity zone splits up and a part of it hits the tongue tip.

The authors noted an intense turbulent kinetic energy production zone in the observed region. The highest values occurred specifically at the trailing edge and at the pressure side of the analyzed blade, as a result of the blade wake. As Figure 17 indicates, a small region of high turbulent kinetic energy stays at the tongue tip as the blade passes close to it.

For a flow rate below the design point (40% of BEP), the PIV method revealed many vortices in the impeller channels. Such vortices promoted the occurrence of recirculation and flow separation. The results thus agree with the observations made by Krause et al. (2006). Nevertheless, for a flow rate above the design point (150% of BEP), the flow was dominated by a single vortex and also conditioned by a detachment from the pressure side of the blade leading edge. As a result, a higher turbulent kinetic energy was produced in that region.

To complete their study, Keller et al. (2014) used a *stereoscopic* PIV, or 2D-3C PIV, to measure the axial component of the velocity vectors. Due to the two-dimensional shape of the pump prototype, however, this axial velocity was limited to 10% of the blade tip velocity. As mentioned in Section 3, the 2D-3C PIV is useful to obtain three-component velocity fields in planar regions. The method is implemented by using two cameras arranged at an oblique angle. The flow images are captured and then processed on a computer to determine the velocity perpendicular to the light sheet.

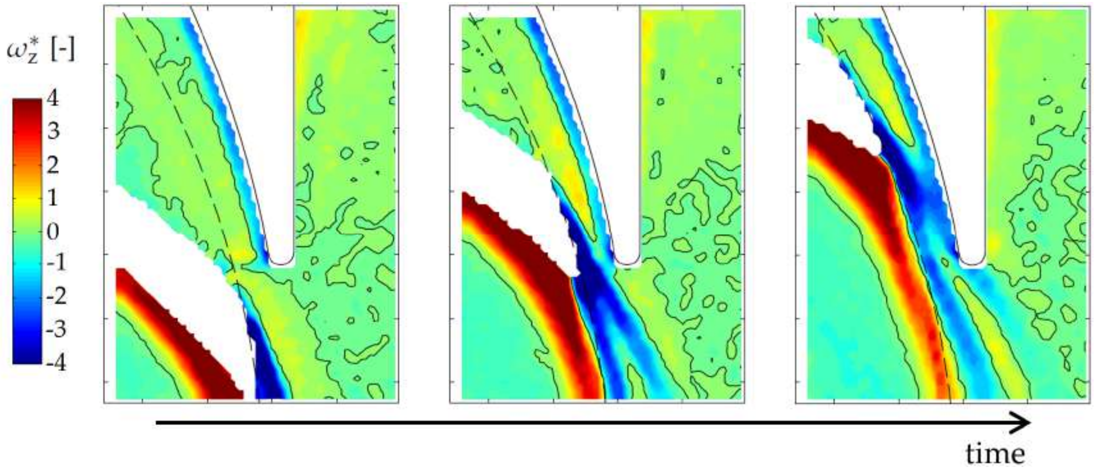

Figure 16. Vorticity (ω^*_z) next to the volute tongue. The impeller rotation sense is counterclockwise. The maximum negative ω^*_z sheet is formed at the blade trailing edge and intercepts the tongue tip. Figure adapted from Keller (2014).

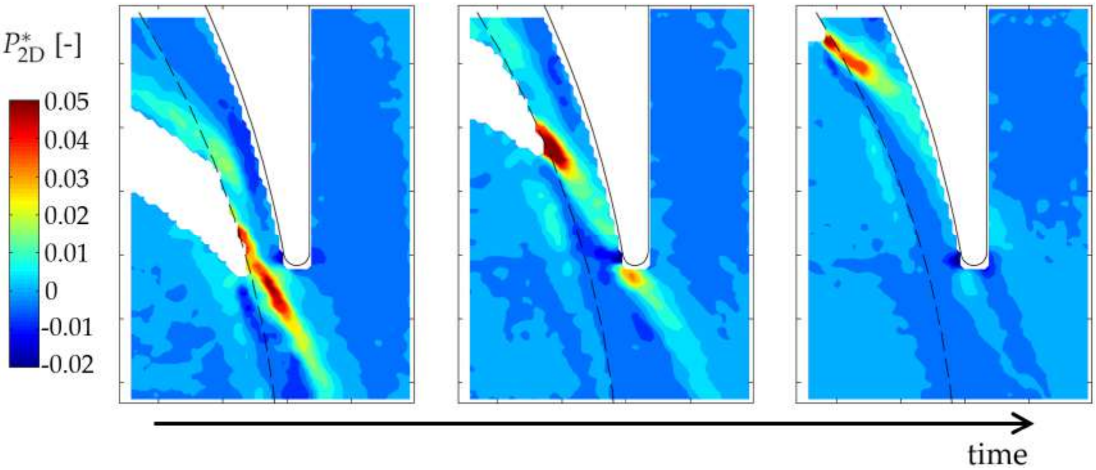

Figure 17. Turbulent kinetic energy production (P^*_{2D}) next to the volute tongue. The maximum P^*_{2D} occurs at blade trailing edge when it aligns with tongue tip. Figure adapted from Keller (2014).

Yang et al. (2012) used a 2D-3C PIV system to investigate a water flow in a radial pump as well. In the tests, the authors measured the axial, radial, and transverse components of the instantaneous velocity vectors in three axial sections of the impeller. The presence of secondary flows was observed in five radial sections of the impeller, between the upper plane (*shroud*) and the lower plane (*hub*). Finally, from the continuity equation, the authors calculated the uncertainties associated with their methodology and found maximum errors of about 3%.

As the previous paragraphs demonstrate, water is generally the fluid preferred by authors who study single-phase flows in pumps. Furthermore, when a PIV technique is used, the authors usually develop pump prototypes made of transparent plastics that enable the entrance of laser light to the impeller and diffuser. This practice was adopted, for example, by Pedersen et al. (2003), Feng et al. (2009), Krause et al. (2006), Keller et al. (2014), and Yang et al. (2012). However, such transparent materials as the acrylic glass have a refractive index of about 1.49, while water has a low refractive index of only 1.33. Such difference usually generates a distortion in the laser sheet that illuminates the flow, a condition that may intensify the uncertainties in the velocity measurements.

In order to solve this issue, Wu et al. (2009, 2011) adopted a practice named as *refractive index matching* (RIM-PIV), which essentially consists of using a fluid with the same refractive index as the material that compose the solid walls. The authors prepared a water solution with 64% by weight of sodium iodide and then performed experiments to obtain streamlines and velocity vectors in the volute and impeller of a pump prototype working at 1000 rpm. The results achieved with RIM-PIV were finally compared with results from the conventional PIV and the authors could conclude that the *refractive index matching* yielded measurements with high quality and low uncertainty. As Section 3 reported, the RIM-PIV indeed reduces the deviations in the laser sheet when it crosses liquid-solid interfaces.

The RIM-PIV method was used by other authors with different fluids. Mittag and Gabi (2016), for example, adopted a methodology combining 2D-3C PIV, TR-PIV, and RIM-PIV to obtain the velocity fields of a single-phase flow at the intake region of a centrifugal pump. Two cameras were employed to configure the *stereo*-PIV system whose *time-resolved* laser source pulsed at a frequency of 2 kHz. With a viscosity of 0.025 Pa.s (25 cP), the Shell Gravex 917 mineral oil was used as the working fluid. Silver coated borosilicate microspheres were added to the oil to act as seeding tracers. According to the authors, as the mineral oil has the same refractive index as the pump housing, the distortions in the laser beam were limited to 0.2% only. As a comparison, distortions would have reached 12.5% if the oil were replaced by water, for example.

Among the most recent publications, the study by Li et al. (2020) stands out. The authors used a conventional PIV technique to visualize the water flow in a centrifugal pump working at 1000 rpm. Figure 18 displays a photograph of the experimental facility during the execution of an experiment, with an emphasis on the laser generator, the high-speed camera, and the transparent prototype.

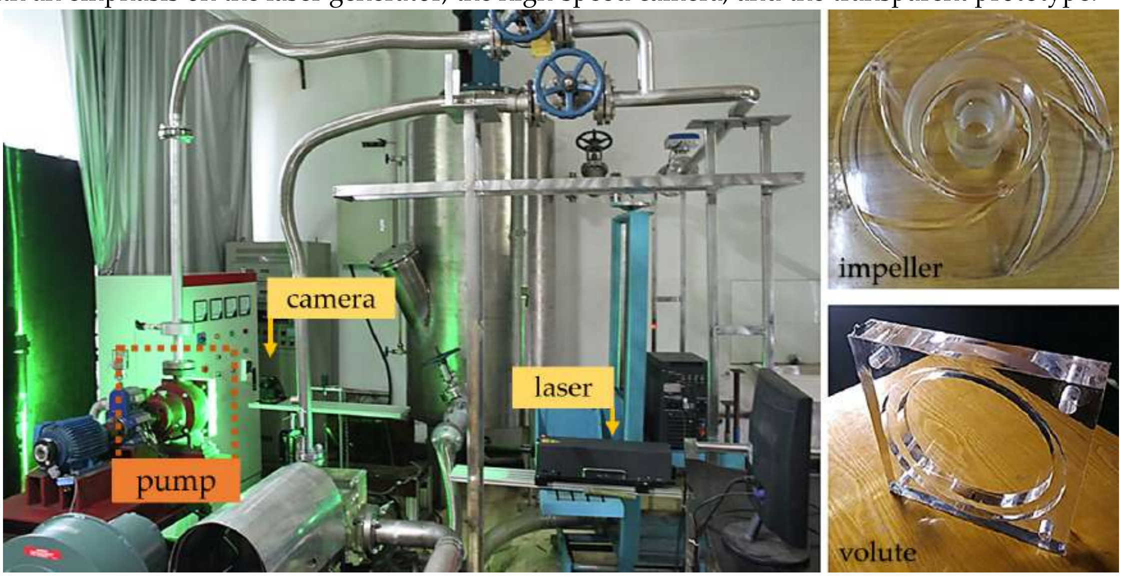

Figure 18. Test facility used to perform 2D-2C PIV experiments. Figure adapted from Li et al. (2020); Reproduced with permission from Renewable Energy; Published by Elsevier in 2020.

The time interval between two laser pulses was defined to correspond to a 0.78° (or 0.014 rad) rotation in the impeller. Eight flow rates were investigated and aluminum oxide particle tracers were added to the water flow. Still, the great innovation of the study by Li et al. (2020) was the possibility of visualizing all five impeller channels simultaneously, an impractical condition in the other studies reported in this section. In fact, the pump prototype developed by Li et al. (2020) was designed in such a way that the position of the pump intake and discharge did not impair the visual access of the camera to the impeller. Consequently, the authors were able to determine velocities and streamlines in the entire impeller front plane, as shown in Figure 19.

As can be observed, Figure 19 indicates that the single-phase flow regime varies significantly depending on the flow rate. Therefore, they are responsible for the performance decrease that occurs when the pump operates away from the design operating condition, or BEP. At the design flow rate, associated with the maximum efficiency (Q_{BEP}), the streamlines tend to follow the same curvature of the blades, a condition that optimizes the transference of energy from the impeller to the fluid flow. However, at partial flow rates, vortices appear in the channels, in a region close to the suction and pressure sides of the blades. These clockwise and counterclockwise vortices influence the velocity profiles and, therefore, impair the energy conversion by the pump. This clear relationship between flow pattern and pump performance was identified by other authors, such as Pedersen et al. (2003), Krause et al. (2006) and Keller et al. (2014), whose studies were reported above.

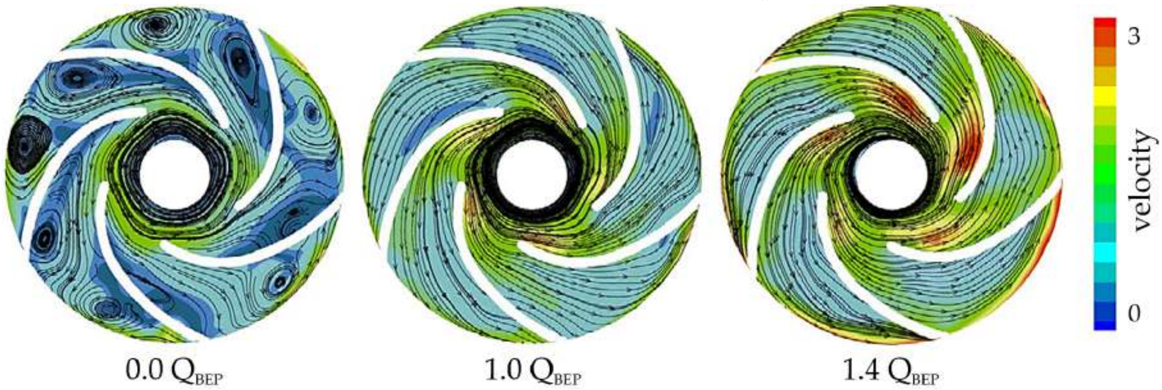

Figure 19. Phase-averaged relative velocity normalized with impeller circumferential velocity. Flow streamlines reveal the presence of vortices at *shut-off* condition. Figure adapted from Li et al. (2020); Reproduced with permission from Renewable Energy; Published by Elsevier in 2020.

In view of the information exposed in this section on the visualization of single-phase flows in centrifugal pumps, it is possible to draw the following conclusions:

- The studies mentioned in the previous paragraphs have great relevance for the advancement of the phenomenological comprehension on single-phase flows in rotating environments, usually subject to intense centrifugal forces, shear stresses, and turbulent structures.
- In all the reported studies, the Nd:YAG laser was used to illuminate the fluids. In general, the authors adopted the traditional PIV (2D-2C PIV), but part of them preferred the *stereoscopic* PIV (2D-3C PIV) with two cameras. The laser pulsation frequency was limited to 100 Hz, although a few authors adopted a *time-resolved* (TR-PIV) technique to perform measurements with a higher frequency in the order of 1000 Hz.
- Most studies focused on water flows. Only a few authors used liquids with the same refractive index as the solid materials, a practice known as *refractive index matching* (RIM-PIV). In addition, only one study investigated the single-phase gas flow, using air as the working fluid.
- In most studies, the authors used glass microspheres as tracers. However, in some cases, it was preferred to add fluorescent seeding tracers to the fluid, in a *laser-induced fluorescence* (LIF-PIV) practice. Polyamide, melamine, acrylic, Al_2O_3 and TiO_2 are among the most selected materials.
- A few authors also performed experiments using LDV and numerical simulations using CFD. PIV methods, however, appeared to have some relevant advantages over the other techniques, as a reduced run time and a greater ability to detect fast flow structures. Hence, PIV has clearly demonstrated to be the most preferred technique for single-phase flow visualization in pumps. (Nevertheless, it should be emphasized that LDV may provide results with superior resolutions when the measurement is performed in regions adjacent to solid walls, where PIV is negatively affected by intense light reflections, for example. In addition, LDV has usually higher accuracy in point measurements, as it is based on Doppler effect and does not require image calibration.)
- All authors investigated the flows inside centrifugal pump prototypes with transparent parts that allowed visual access to their interior. In most studies, only one impeller channel could be visualized, so that a single study was able to analyze the entire impeller at once. In the studies

reported in this section, the diameters of the impellers ranged from 27 millimeters (the smaller inner diameter) to 556 mm (the larger outer diameter).

- In general, these impellers worked at rotations lower than the nominal ones recommended by the pump manufacturers. In most studies, these rotations were in a range from 500 to 1000 rpm, while only one study could reach a speed higher than 1500 rpm. This finding may suggest that the experimental facilities possibly have technical limitations that restrict the authors to study low rotational speeds. On the one hand, the PIV system may have limited resolutions, possibly insufficient to measure fast flows in rotating environments. On the other hand, the transparent pump prototype may have a fragile structure, which is damaged when the rotation is too high.
- All the studies reviewed so far have focused their efforts on investigating single-phase flows in radial pumps. Other pump types, although quite common in industrial applications, have not been studied with respect to flow visualization. This fact demonstrates the difficulty of using a PIV method to perform measurements in mixed and axial impellers, for example, in which the flow is three-dimensional. The geometry of a mixed or axial impeller actually impairs the access of both laser and camera to the interior of the channels.
- As a first result, the studies determined the velocity fields in different parts and regions of the centrifugal pumps. The measurement of these velocity vectors allowed the authors to obtain streamlines, vorticity estimates, turbulence kinetic energy maps, among other relevant results.
- The studies reported in this section make evident the dependence between the velocity fields in the impellers and the performance of the centrifugal pumps. In flow rates other than the design points, the occurrence of wakes, jets, vortices, and recirculation zones was clearly identified by the authors, who attributed such mechanisms to the reduction of the pump capacity to transfer energy from the impeller to the fluid.

The studies reviewed throughout this section are summarized in Table 2.

Table 2. Summary of studies reviewed on the visualization of single-phase liquid flows.

Authors	Methods	Fluids and particle tracers	Region analyzed and pump type	Main results achieved
Wuibaut et al. (2002)	2D-2C PIV.	Air; polyethylene glycol particles.	Impeller and volute of transparent radial centrifugal pump.	Velocity curves as function of positions. Maps with fluctuation rate.
Pedersen et al. (2003) and Pedersen (2000)	2D-2C PIV, LIF-PIV, LDV.	Water; melamine resin particles, rhodamine dye.	Impeller of 2-stage radial centrifugal pump.	Velocities as function of positions and flow rates. Turbulent kinetic energy.
Feng et al. (2009)	2D-2C PIV, LDV, CFD.	Water; polyamide.	Impeller and diffuser of transparent radial centrifugal pump.	Radial and transverse velocities. Maps with turbulent intensity.
Krause et al. (2006)	2D-2C PIV, LIF-PIV, TR-PIV.	Water; melamine resin particles, rhodamine dye.	Impeller of a transparent radial centrifugal pump.	Velocity as function of time. Flow streamlines. Detection of vortices.
Gerlach (2018)	2D-2C PIV.	Water; titanium dioxide powder.	Impellers with various geometric shapes and diameters.	Velocity. Vorticity. Pump performance as a function of impeller characteristics.
Keller et al. (2014) and Keller (2014)	2D-2C PIV, LIF-PIV.	Water; hollow glass microspheres, fluorescent tracers.	Impeller and volute of transparent radial centrifugal pump.	Velocity. Vorticity. Turbulent kinetic energy. Frequency spectrum.
Yang et al. (2012)	2D-3C PIV.	Water; aluminum oxide.	Impeller of a transparent radial centrifugal pump.	Velocity curves. Detection of secondary flows. Estimation of uncertainties.

Wu et al. (2009, 2011)	2D-2C PIV, LIF-PIV, RIM-PIV.	Sodium iodide and water mixture, fluorescent tracers.	Impeller and volute of transparent radial centrifugal pump.	Comparison of results: LIF-PIV with RIM-PIV *versus* 2D-2C PIV.
Mittag and Gabi (2016)	2D-3C PIV, RIM-PIV, TR-PIV.	Oil; silver coated hollow glass microspheres.	Intake region and impeller of centrifugal pump.	Velocity profiles. Flow streamlines. Maps with flow rates.
Li et al. (2020)	2D-2C PIV.	Water; aluminum oxide.	All impeller channels of a transparent radial centrifugal pump.	Velocities as function of positions and flow rates. Streamlines. Vortices.

4.2. Two-Phase Flows in Centrifugal Pumps

As explained in Section 2, the performance of a centrifugal pump is seriously impacted when gases or viscous fluids enter its impellers and diffusers. The presence of free gas reduces the pump ability to transfer energy from the impeller to the fluids, a condition that causes a severe decrement in the device performance. Likewise, the presence of dispersions and emulsions with high viscosities intensifies friction losses and promotes an increase in the power required by the pump, factors that engender a drastic reduction in its efficiency. Figure 20 illustrates the head degradation in two real pumps in effect of gas fraction and liquid viscosity increments.

In the petroleum industry, the production of viscous oils by the Electrical Submersible Pumping systems demands the use of oversized equipment, which consume high levels of energy and thus reduce the well profitability. In the case of pumping two-phase gas-liquid and liquid-liquid flows, the unexpected occurrence of transient phenomena, such as *surging* and *phase inversion*, represent operational issues characterized by fluctuations in the electric motor load, whose direct consequence is a decline in the service life and reliability of the entire system (Monte Verde et al., 2017; Morales et al., 2012; Bulgarelli et al., 2020a; Bulgarelli et al., 2020b; Hartenbach et al., 2015; Honório et al., 2015).

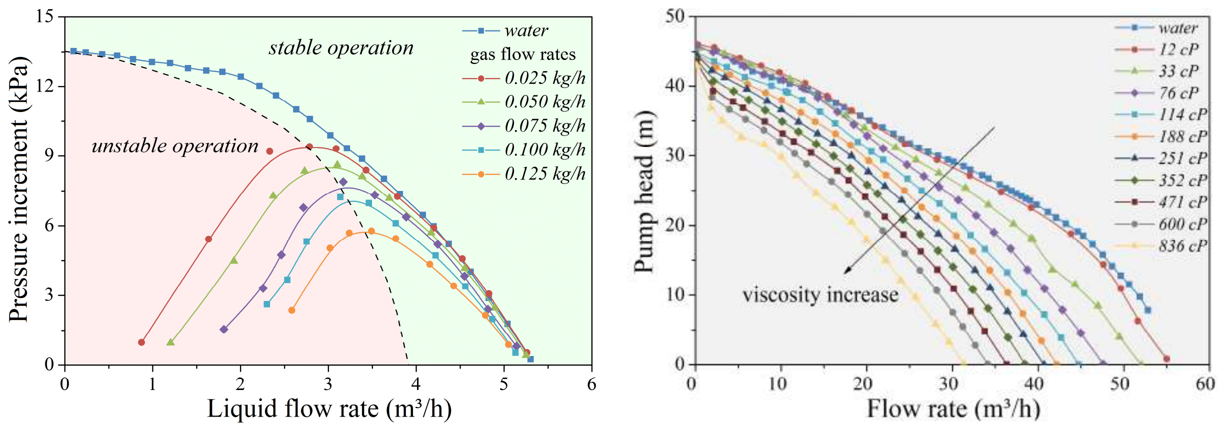

(**a**) two-phase air-water flow (**b**) single-phase water-glycerol flow

Figure 20. Curves of Δp and H as functions of Q for (a) 1-stage *GE Baker-Hughes Centrilift 538 P23* and (b) 3-stage *Schlumberger GN 5200* pumps. As the gas fraction or mixture viscosity increase, the pump performance decreases. Figure adapted from Monte Verde (2016).

In this framework, the execution of flow visualization experiments is imperative to improve the understanding of the relationship between the pump performance and the flow pattern observed in its impeller. A set of studies that represent the state-of-the-art on this topic are reported in the next sections, 4.2.1 and 4.2.2, with discussions on strengths and weaknesses of visualization techniques, contributions and limitations of main results achieved, comparisons between interpretations made by experts, as well as suggestions for future researches.

4.2.1. Gas-Liquid Flows

The initial studies on gas-liquid flows were motivated by the nuclear power industry, in which centrifugal pumps were used in reactor cooling systems and, therefore, there was extreme concerns about the risk of leakage of radioactive fluids. In this sense, decades ago, Murakami and Minemura (1974a, 1974b) studied the performance of pumps working in presence of water and air for purposes related to the use in nuclear powerplants, a topic that was later investigated by other authors, such as Sato et al. (1996), Poullikkas (2003), and Thum et al. (2006), for example.

One of the first studies on the dynamics of gas bubbles inside a pump impeller was published by Minemura and Murakami (1980). In a two-phase air-water flow, they concluded that three forces govern the motion of bubbles, in a referential fixed to the pump housing: drag force imposed by water, pressure force due to gradient in the impeller channel, and inertial force named *virtual mass*. Recently, new studies were conducted by Perissinotto et al. (2017), Stel et al. (2019), and Cubas et al. (2020). Visualization techniques based on *Particle Tracking Velocimetry* allowed these researchers to follow individual bubbles in the flow images in order to quantitatively evaluate their dynamics in pump impellers.

Within the scope of the petroleum industry, the effects of the presence of free gas in centrifugal pumps were already discussed by Lea and Bearden (1982) decades ago. However, a pioneering work on visualization of bubbles was achieved by Estevam (2002), with focus on the analysis of gas-liquid flows in ESP systems. The researcher developed a prototype with a transparent impeller in which he identified the formation of a population of stationary air bubbles responsible for reducing the pump performance due to the surging phenomenon. The author proposed a model based on dimensionless numbers to predict the flow pattern observed inside the impeller for each operational condition.

Researchers who study centrifugal pumps agree that their operation is severely impacted by the presence of gas. In recent years, several studies have been published to assess the effects of variables such as rotational speed, intake pressure, and gas fraction on the pump performance. Some authors also employed the *High-Speed Imaging* as a visualization technique in order to identify patterns in two-phase gas-liquid flows and relate them to the reduction of the pressure generated by the pumps. Gamboa and Prado (2010), Trevisan and Prado (2010, 2011), Barrios and Prado (2011a, 2011b), Zhang et al. (2016), Monte Verde (2016), Monte Verde et al. (2017), Shao et al. (2018), and Zhao et al. (2021) are relevant examples.

Barrios and Prado (2011a, 2011b) analyzed the two-phase air-water flow within the impeller of a transparent prototype developed by Barrios (2007). They used a high-speed camera as visualization method to examine the behavior of both phases under various flow conditions. The authors could conclude that the degradation of pump performance was related to the formation of larger bubbles, classified as a *gas pocket* type, which caused a partial blockage in the impeller channels. Figure 21 shows the pump prototype and a population of air bubbles observed with the HSI method.

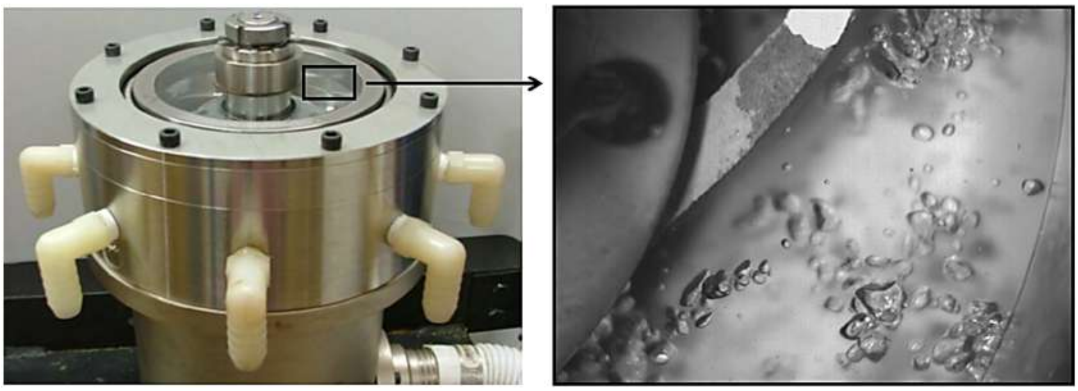

Figure 21. Visualization of gas bubbles in a two-phase air-water flow within an impeller. The pump has a transparent window that enables visual access to the flow. Figure adapted from Barrios (2007).

Barrios and Prado (2011a, 2011b) proposed a mechanistic model comprising a one-dimensional force balance that predicts the occurrence of stagnant gas bubbles at the channel intake. The model indicates the transition to surging, a condition related with operational instability and performance degradation. Besides, *Computational Fluid Dynamics* (CFD) simulations were carried out by Barrios (2007) and the results were consistent with the data collected during the experiments.

Zhang et al. (2016) developed a three-stage prototype with axial impellers and transparent parts made of acrylic glass in order to study the effects of a two-phase air-water flow on its performance. A high-speed camera with a resolution of 1280x1024 pixels and acquisition rate of 5000 frames per second (fps) was used to visualize the flow. The authors identified four flow patterns, classified as *isolated bubble flow*, *bubbly flow*, *gas pocket flow*, and *segregated flow*. According to Zhang et al. (2016), the bubbles in the impeller are affected by pressure gradients, drag force, centrifugal force, Coriolis force, and buoyancy, considering that the mixture is in a state of thermodynamic equilibrium, at a constant temperature, and without mass and heat transfers. The centrifugal force is generated by the impeller rotation and it is directed outward, along the radius, while the drag force is produced by the liquid velocity, which tends to be higher than the gas velocity.

Similarly, Gamboa and Prado (2010) conducted two-phase air-water flow visualization tests using a high-speed camera and a two-stage centrifugal pump prototype with a transparent housing. The authors identified three flow patterns in the pump impeller: *bubbles*, *elongated bubbles*, *blockage*, the last one being characterized by the presence of a *gas pocket*, as shown in Figure 22. Flow images revealed that the gas injection point changes the pump performance: on the one hand, when the air is injected at the entrance of the first stage, many bubbles reach the impeller with approximately 500 micrometers in diameter; on the other hand, when the air is injected at the second stage, the bubbles exhibit larger diameters up to 3.5 millimeters, a growth that drastically reduces the ESP efficiency.

The influence of gas density and gas-liquid surface tension on the pump performance was also examined by Gamboa and Prado (2010), who used isopropanol and sulfur hexafluoride (SF_6) in their experiments. The former is an alcohol whose surface tension is one third of air-water surface tension, and the latter is a gas whose density is six times the air density at 20°C. The SF_6-water flow revealed a direct dependence of the pump performance on the gas density: the denser the gas, the greater the void fraction needed to impair the pump behavior. In the opposite way, the air-water/isopropanol mixture indicated that surface tension and pump performance are inversely proportional: a higher alcohol concentration means a lower surface tension, which facilitates bubble fragmentation and, as a consequence, improves the pump ability to handle free gas.

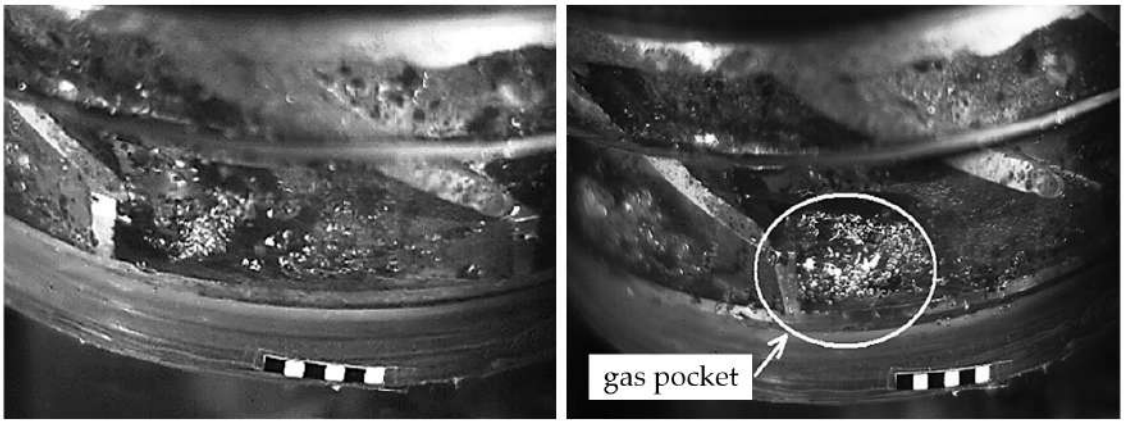

Figure 22. Transition from bubbles to gas pocket in an impeller at 600 rpm. The gas volume fraction is about 1%. When the gas pocket flow is formed, the pressure generated by the pump decreases 80%. Figure adapted from Gamboa and Prado (2010).

In parallel with Gamboa and Prado (2010), the studies done by Trevisan and Prado (2010, 2011) evaluated the influence of the viscosity on the performance of a transparent prototype working with two-phase air-water and air-oil flows. The void fraction was up to 5% while the oil viscosity varied from 46 to 161 centipoise (cP). With an HSI method, the researchers observed five patterns in the impeller channels, depending on the liquid viscosity and gas fraction: *dispersed bubbles*, *agglomerated bubbles*, *gas pockets*, *segregated gas*, and *intermittent gas*. The authors claimed that the agglomerated bubbles pattern was responsible for an initial pump head degradation and the gas pocket structures coincided with the occurrence of surging events. Therefore, they concluded that the liquid viscosity changes the size and shape of the gas bubbles which, consequently, cause surging to occur at lower void fractions.

Most of the experimental observations made by Barrios and Prado (2011a, 2011b), Gamboa and Prado (2010), and Trevisan and Prado (2010, 2011) were repeated and/or extended by Monte Verde (2016) and Monte Verde et al. (2017). The PhD thesis elaborated by Monte Verde (2016) is actually a very complete study on two-phase gas-liquid flows in centrifugal pumps available in the literature. The author worked on two experimental facilities with the objective of improving his understanding on the factors that influence the performance of pumps used in ESP systems. To visualize the flows, the researcher designed and built a pump prototype that allowed a visual access to the interior of its impeller channels, through a transparent shroud made of acrylic material. Then, using a high-speed camera with an acquisition rate of 2000 fps at the maximum resolution of 1280x1024 pixels, Monte Verde (2016) identified four patterns in a two-phase air-water flow, which received the following nomenclature: *bubble flow*, *agglomerated bubble flow*, *gas pocket flow*, and *segregated flow*, as Figure 23 shows. The results were published in a scientific paper by Monte Verde et al. (2017).

According to Monte Verde et al. (2017), the *bubble flow* pattern is observed only for extremely low air fractions and consists of small dispersed bubbles. The *agglomerated bubble flow* pattern occurs after an increment in the air fraction, which increases the population and size of the air bubbles. A larger number of bubbles implies a more frequent interaction between them, with the development of agglomeration and coalescence events. As the air fraction continues to increase, the *gas pocket* flow pattern is established, characterized by a large bubble with a deformable and unstable interface. This bubble blocks a considerable volume of the impeller channels and, consequently, reduces the energy conversion from the impeller to the fluids, leading to a degradation of the pump performance. This condition typically promotes the occurrence of surging phenomena. Then, the *segregated flow* pattern, which occurs for even larger air fractions, consists in the growth of the gas pockets, which begin to occupy the entire volume of the channels. In this case, due to the complete blocking of the impeller, the pump becomes unable to transfer energy to the fluids, a condition named as *gas locking*.

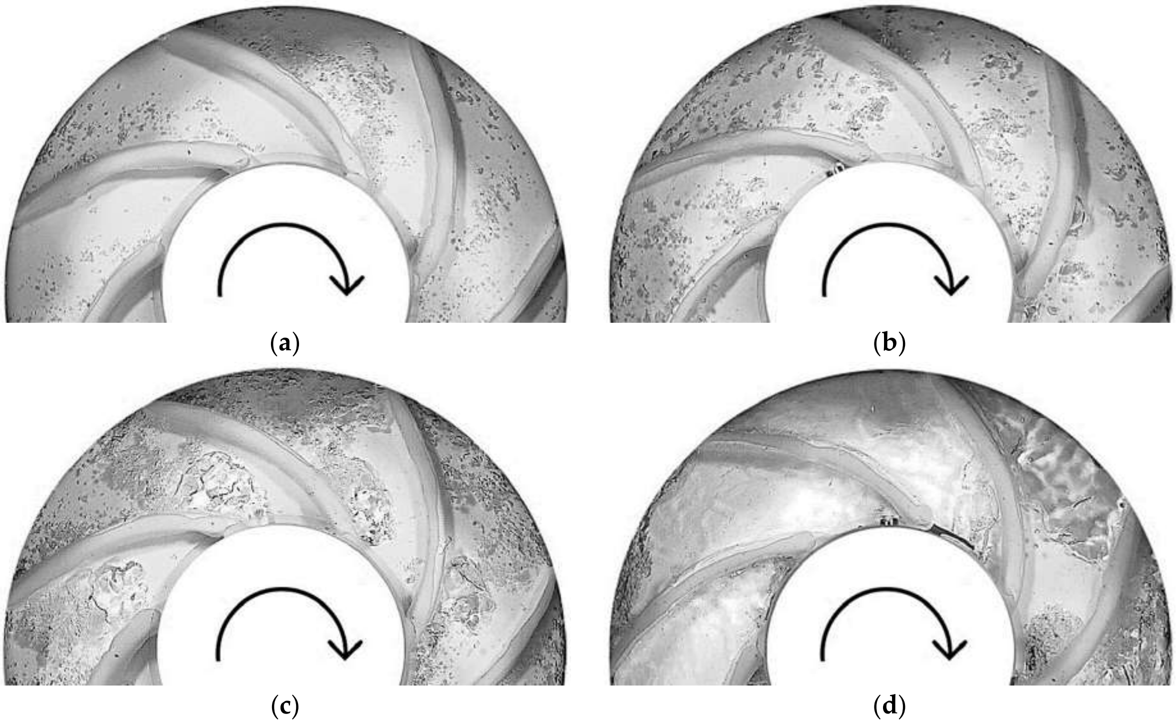

Figure 23. Air-water flow patterns in pump impeller: (a) bubble flow; (b) agglomerated bubble flow; (c) gas pocket flow; (d) segregated flow. Impeller rotates at 900 rpm, gas flow rate is 0.050 kg/h, gas volume fraction varies from 0.6 to 2.5%. Figure adapted from Monte Verde et al. (2017); Reproduced with permission from Experimental Thermal and Fluid Science; Published by Elsevier in 2017.

Monte Verde (2016) repeated their experiments with air-water/glycerol mixtures and observed that viscosity is detrimental to pump performance. In fact, viscous liquids intensify the process of growth and coalescence of gas bubbles in the impeller channels, causing the segregated flow pattern to occur prematurely. An increase in viscosity, thus, decreases the pump tolerance to the presence of gas. Monte Verde (2016) finally performed tests with air-water/isopropanol mixtures and discovered that a reduction in the surface tension is beneficial for the pump. In effect, a low gas/liquid surface tension facilitates the fragmentation of the gas bubbles, which tend to remain small and dispersed, maintaining the bubble flow pattern even at higher gas fractions. Figure 24 illustrates the qualitative differences between air-water, air-water/isopropanol, and air-water/glycerol mixtures at a constant air fraction.

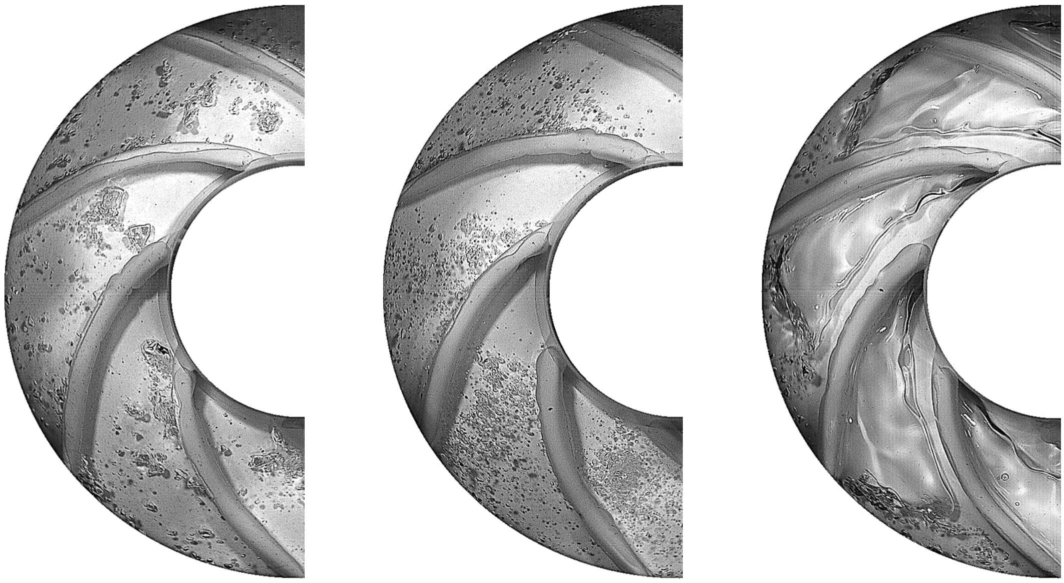

(**a**) (**b**) (**c**)

Figure 24. Two-phase gas-liquid mixtures in impeller: (a) air-water flow with viscosity μ = 1 cP and surface tension σ = 72 mN/m; (b) air-water/isopropanol flow with σ = 53 mN/m; (c) air-water/glycerol flow with μ = 20 cP. The impeller rotates at 900 rpm. The inlet gas volume fraction is constant at 0.5%. Figure adapted from Monte Verde (2016).

The results achieved by Monte Verde (2016) were used to model the performance parameters of a three-stage radial pump operating with viscous fluids, based on a methodology developed from the slip model by Zuber and Findlay (1965). The approach had been previously adopted by Biazussi (2014) for air-water flows in order to represent the pump head and shaft power in three commercial models of pumps used in ESP systems. In general, there was excellent agreement between the data obtained from the experiments and the results calculated from the proposed models, both in the case of Monte Verde (2016) and Biazussi (2014).

The paper by Zhu and Zhang (2018) contains a wide review of the main experiments carried out and models developed in recent years within the scope of two-phase gas-liquid flows in centrifugal pumps. The review article has a great relevance for the petroleum industry. Among the most recent publications, it can be cited the studies by Shao et al. (2018) and Zhao et al. (2021), who investigated an air-water flow in the impeller and volute of transparent centrifugal pumps.

The studies reported in this section reveal that the visualization of two-phase gas-liquid flows in centrifugal pump impellers is usually performed in prototypes produced with transparent parts. Besides, the use of *High-Speed Imaging* and *Particle Tracking Velocimetry* is an interesting strategy to identify flow patterns (e.g. Gamboa and Prado, 2010; Monte Verde et al., 2017) and track gas bubbles immersed in liquids (e.g. Zhang et al., 2016; Perissinotto et al., 2017) to estimate variables associated with their motion. According to Thoroddsen et al. (2008) and Mohammadi and Sharp (2013), flow visualization using high-speed cameras has numerous advantages, since these devices guarantee the observation of fast transient phenomena with high spatial and temporal resolutions.

The studies reviewed throughout this section are summarized in Table 3.

Table 3. Summary of studies reviewed on the visualization of two-phase gas-liquid flows using HSI.

Authors	Two-phase gas-liquid flow	Pump type	Operational parameters varied	Main results achieved and parameters investigated
Estevam (2002)	Air-water.	Transparent pump prototype (1 stage), centrifugal pump (2 stages).	Gas fraction, liquid flow rate, impeller rotation speed.	Flow images. Pump performance. Model to predict the flow pattern in the pump impeller.
Barrios and Prado (2011a, 2011b) and Barrios (2007)	Air-water.	Transparent pump prototype (2 stages). Radial impeller.	Gas fraction, liquid flow rate, impeller rotation speed.	Flow images and patterns. Pump performance. Size, shape, path, and dynamics of bubbles.
Zhang et al. (2016)	Air-water.	Transparent pump prototype (3 stages). Axial impeller.	Gas fraction, liquid flow rate, impeller rotation speed.	Flow images and patterns. Pump performance. Size, shape, path, and dynamics of bubbles.
Gamboa and Prado (2010)	Air-water; SF_6-water; air-water/isopropanol. (SF_6 = sulfur hexafluoride)	Transparent pump prototype (2 stages). Mixed impeller.	Rotation, flow rate, gas injection point, isopropanol fraction.	Flow images and patterns. Effects of gas density, injection point, and surface tension on pump performance.
Trevisan and Prado (2010, 2011)	Air-water and air-oil.	Transparent pump prototype (2 stages). Mixed impeller.	Rotation, flow rate, oil temperature.	Flow images and patterns. Effects of viscosity on pump performance.
Monte Verde et al. (2017) and Monte Verde (2016)	Air-water; air-water/glycerol; air-water/isopropanol.	Transparent pump prototype (1 stage), ESP pump (3 stages). Radial impeller.	Gas fraction, liquid flow rate, impeller rotation speed, intake pressure, inclination angle.	Flow images and patterns. Influence of inclination, pressure, viscosity, and surface tension. Models for viscous correction and for performance analysis.
Shao et al. (2018)	Air-water.	Transparent pump prototype (1 stage). Radial impeller.	Gas fraction, liquid flow rate, impeller rotation speed.	Flow images. Pump performance. Motion of gas bubbles.
Zhao et al. (2021)	Air-water.	Transparent pump prototype (1 stage). Radial impeller.	Gas fraction, liquid flow rate, impeller rotation speed.	Flow images and patterns. Pump performance. Behavior of gas bubbles.

Recently, new non-intrusive visualization techniques have started to be used for the analysis of two-phase flows in impellers. An important method is *Computed Tomography* (CT) which works with gamma-ray (or γ-ray) and x-ray radiations. Bieberle et al. (2007), Hasaan et al. (2008), Duplaa et al. (2013), Neumann et al. (2016), Schäfer et al. (2015, 2017, 2020) are examples of authors who used CT to measure the gas holdup in pumps. The main advantage of CT over other methods, such as HSI and PIV, is the possibility of being applied in real pumps with metallic housings. In other words, as the radiation can penetrate opaque materials, the CT technique does not demand the development of transparent prototypes. This fact is illustrated in Figure 25, which shows radiographic scans of a real pump, *KSB Etachrom BC C11* model, operating at 1480 rpm with an entrainment gas volume fraction of 4%.

The spatial and temporal resolutions of CT systems have greatly increased in recent years due to technological advances in digital data processing and radiation sources and detectors. Therefore, CT imaging techniques have become an interesting approach of highest potential to quantitatively determine gas holdup distributions in rotating machines and their components. In this context, the capability of γ-ray and x-ray CT methods to disclose the behavior of a transient gas-liquid flow was demonstrated in two recent studies by Schäfer et al. (2017, 2020). As Figure 26 reveals, the authors were able to identify regions in the impeller where the gas phase tended to accumulate. However, the detection of flow structures, as gas pockets and bubbles, was done indirectly since there was no visual access to the flow in the pump.

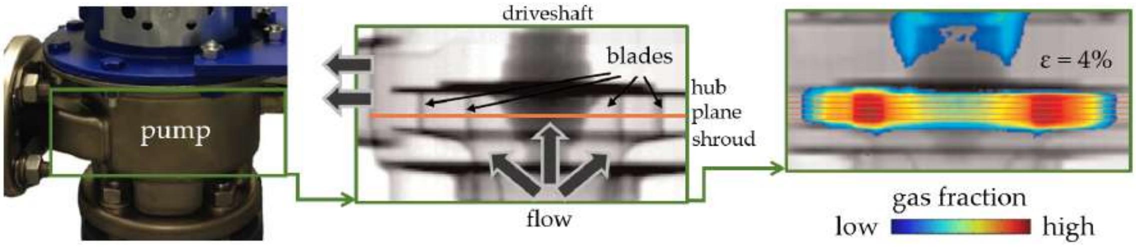

Figure 25. Non-intrusive gamma radiography showing internal components of a centrifugal pump working with two-phase air-water flow. At a gas volume fraction $\varepsilon = 4\%$, the CT reveals that the gas phase stays accumulated in the impeller. Figure adapted from Schäfer et al. (2015); Reproduced with permission from Flow Measurement and Instrumentation; Published by Elsevier in 2015.

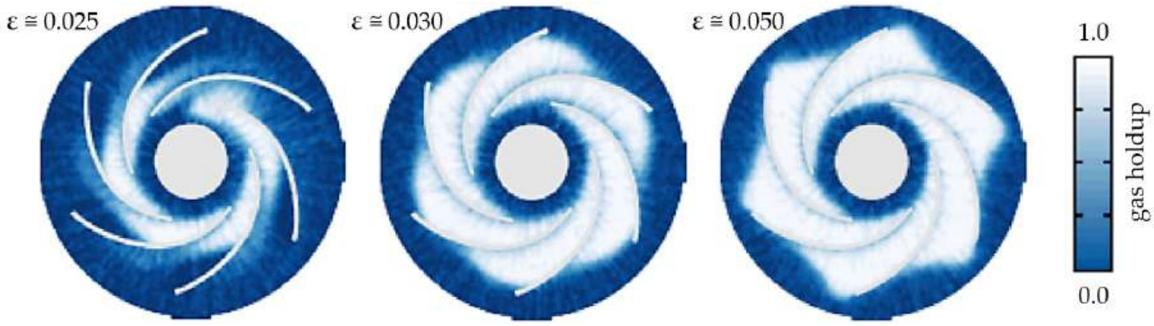

Figure 26. A γ-ray scan showing characteristic structures of air-water distribution in pump impeller rotating at 1480 rpm. The gas holdup is measured as function of the entrainment gas volume fraction. Figure adapted from Schäfer et al. (2017); Reproduced with permission from Nuclear Engineering and Design; Published by Elsevier in 2017.

The images obtained by Schäfer et al. (2017) with CT in Figure 26 are quite different from those obtained by Gamboa and Prado (2010) and Monte Verde et al. (2017) in Figure 22 and Figure 23 with HSI. There is an important limitation of CT in comparison to HSI: the ability to fully visualize the flow down to its tiniest details. Hence, high-speed cameras are generally preferred when gas bubbles must be carefully investigated with respect, for example, to their characteristic size, geometric shape, interface with liquid phase, motion, among other attributes and phenomena that cannot be observed directly with CT methods.

4.2.2. Liquid-Liquid Flows

Two-phase liquid-liquid mixtures may affect the performance of centrifugal pumps by reason of the typical formation of dispersions and emulsions with high effective viscosities. Conceptually, the *effective viscosity* is an average viscosity "felt" by the system when it is pumping a mixture (Kokal, 2005). The mathematical modeling of this viscosity is a challenge for the researchers who work with two-phase liquid-liquid flows. Einstein (1906, 1911) pioneered the creation of an empirical model for predicting the effective viscosity in pipes, followed by other authors such as Vand (1948), Brinkman (1952), Krieger (1972), and Yaron and Gal-Or (1972). Nevertheless, the development of rheological models suitable for being used in centrifugal pumps is incipient, with few studies available in the literature.

Examples should include the studies by Banjar and Zhang (2019) and Croce and Pereyra (2020), who proposed a novel rheological model for effective viscosity and validated it with experiments at the University of Tulsa, using a real ESP with 7 stages. The authors concluded that the model works satisfactorily for medium viscosity emulsions, but offers considerable deviations for low viscosity emulsions. The new emulsion rheology model was then incorporated by Zhu et al. (2019a, 2019b) to create a comprehensive mechanistic model for boosting pressure of centrifugal pumps in operation with water-oil mixtures. In comparison with experimental data obtained by Solano (2009) and Banjar (2018), the deviations were limited to 15%, a number which clearly suggests that the performance model is capable of providing reliable results.

Another common condition that occurs when an ESP system lifts a liquid-liquid dispersion is the *phase inversion*. This transient phenomenon is defined as the conversion of one type of emulsion into another, e.g., from oil-in-water to water-in-oil, or vice versa. The process of a phase inversion depends on the fraction of the fluids that compose the mixture, namely, the oil fraction and also the water fraction, popularly known as *water cut*. In fact, petroleum engineers usually invert water-in-oil emulsions (water dispersed in continuous oil phase) into oil-in-water (oil dispersed in continuous water phase), by adding water to oil, with the intention of reducing the effective viscosity and thus improving the pump efficiency. However, the sudden change in the emulsion viscosity may cause a catastrophic result for the ESP, with a generation of severe operational instabilities (Bulgarelli et al., 2020a; Bulgarelli et al., 2020b). The determination of inversion points in liquid-liquid dispersions was accomplished by Yeh et al. (1964), Arirachakaran et al. (1989), Nädler and Mewes (1997), and Brauner and Ullmann (2002), who proposed mathematical models for use in pipes. Nevertheless, the literature on centrifugal pumps is quite limited and has few publications.

A relevant example is the study by Pavlov and Sannaes (2012), who identified phase inversion points in a real ESP with 84 stages, *Baker-Hughes 538 - P75 SXD* model, installed on an experimental facility with more than 200 meters of pipes. The authors prepared mixtures with five types of oil and varied the flow rates and temperatures to modify the effective viscosity of the water-oil emulsions. The researchers observed that the phase inversion depends on the oil viscosity and water cut. They concluded that the most intense degradation of the pump performance occurs when the emulsion has the continuous phase composed by oil with a low viscosity and the dispersed phase formed by water with a high water cut.

In general, the investigation of two-phase liquid-liquid flows in centrifugal pumps depends on the characterization of the drops dispersed in the impeller, since there is a relationship between the drop average diameter and the pump performance. Measuring the characteristic size distribution of liquid drops which compose an emulsion is a great challenge, since these drops generally have very small diameters, in the order of micrometers. Therefore, the study of liquid-liquid flows sometimes relies on particle analyzers based on laser (e.g. Ibrahim and Maloka, 2006; Khalil et al., 2006; Khalil et al., 2008), ultrasound (e.g. Morales et al., 2012), and optical measurements (e.g. Schäfer et al., 2019; Schmitt et al., 2021).

One of the first studies on drop size measurement in pumps was made by Ibrahim and Maloka (2006), who obtained size distributions for oil-in-water dispersions using a *Laser Particle Size Analyzer* (LPSA). The device consists of a laser emitter and a laser receiver: when the emitted light reaches a drop, a diffraction pattern is formed on the receiver. The amount of diffracted light is dependent on the size of the illuminated drop, which is then estimated.

Similarly, Khalil et al. (2006) used a LPSA device in order to measure drop size distributions in oil-in-water dispersion composed of water and mineral oil, in configurations with surfactants (stable emulsion) and without surfactants (unstable emulsion). These fluids were then used by Khalil et al. (2008) to investigate the performance of a pump operating with two-phase liquid-liquid flows. The authors concluded that the addition of surfactants increases the dispersion viscosity and, as a result, intensely impairs the pump performance.

Morales et al. (2012) analyzed the formation of oil drops in oil-in-water dispersions in a pump. The sizes of the oil drops were measured at the centrifugal pump outlet with an *Ultrasonic Extinction Spectrometer* (UES). The device generates and detects ultrasound: when the waves reach a drop, they are extinct at a frequency dependent on the drop size. The data revealed that the drop size depends on the impeller rotation speed, but it is neither influenced by the mixture flow rate nor by the water cut. Thus, for a continuous water phase, the authors claimed that turbulence is the main mechanism for the fragmentation of oil drops, a conclusion that allowed the development of a new mechanistic model to estimate the diameter of oil drops according to the pump operation conditions.

Recently, new approaches have started to be used for the analysis of particle size distributions. The *Optical Multimode Online Probe* (OMOP) is an important example of a shadowgraphic imaging device which detects boundaries due to differences in contrast between particles and background. It consists of two probes: a camera on one side; a light on the other side; and lenses between them. The device was used by Schäfer et al. (2019) and Schmitt et al. (2021) to evaluate the diameters of oil and water drops, upstream and downstream of centrifugal pumps. The images were processed with a convolutional neural network procedure, which worked properly for drops with sizes larger than 100 μm. An *Endoscope Measuring Probe* (EMP), composed of a camera with superior spatial resolution (1 pixel = 3.5 μm), was finally used for image acquisition at the discharge nozzle of a transparent pump. Thus, the authors were able to analyze the drop break-up phenomena at this static region of the pump, and also to develop new correlations from their observations.

Figure 27 contains examples of images acquired with OMOP and EMP.

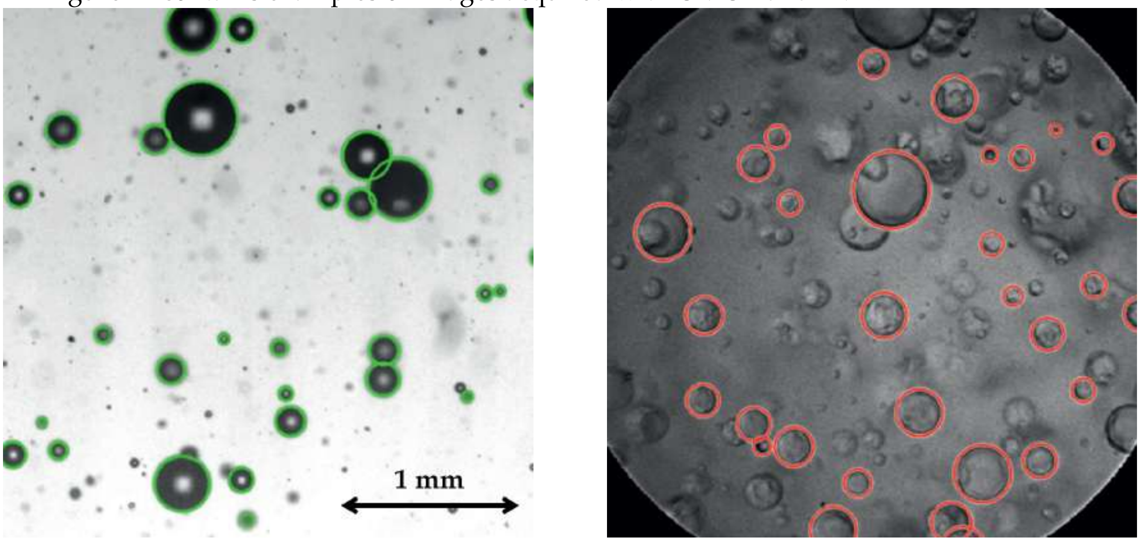

(**a**) OMOP (**b**) EMP

Figure 27. Characteristic sizes of dispersed drops measured with: (a) shadowgraphic imaging device, OMOP; and (b) endoscopic device, EMP. The figure was adapted from Schmitt et al. (2021).

As discussed in the paragraphs above, although LPSA and UES are two powerful strategies for measuring the size of dispersed drops, the devices cannot actually visualize the flow. Such limitation is overcome using OMOP and EMP devices, which have embedded cameras to capture flow images. However, as these particle analyzers are installed at the pump inlet or outlet, they can visualize the emulsion before or after it passes through the pump, but they cannot visualize the emulsion when it is moving inside the rotating impeller. Besides, these devices usually have limited spatial resolutions which may be insufficient to detect small details in the mixtures.

Thus, an alternative approach to visualize emulsions to their tiniest details is *Optical Microscopy* (OM). The technique was used by Bulgarelli (2018) and Valdés et al. (2020) to identify the shapes and sizes of dispersed drops. The main advantage of OM over other methods is the ability to visualize very small drops, with diameters below 10 μm, which would be impossible to detect with cameras. However, OM has the same limitation as OMOP and EMP, i.e., the visualization must be performed out of the impeller. In the case of OM, an emulsion sample must be extracted from the experimental apparatus and placed on the optical microscope to be correctly analyzed.

Figure 28 contains examples of images acquired with OM.

Together with OM, Bulgarelli (2018) used a method called *Focused Beam Reflectance Measurement* (FBRM), which essentially works as an LPSA technique. The researcher determined the chord length distribution of water drops, which presented a spherical geometry with diameters between 1 and 100 micrometers. In fact, the master's dissertation by Bulgarelli (2018) stands out as a broad study on the performance of centrifugal pumps operating with liquid-liquid dispersions. The author carried out experiments at several rotational speeds (800 to 3500 rpm) and oil viscosities (40 to 300 cP) in a real ESP with 8 stages, *Baker-Hughes 538 - P100 L* model. Bulgarelli (2018) concluded that the pump strongly contributes to the formation of emulsions, because the drop size decreases as the impeller rotational speed increases, in a condition that directly favors the increment of the effective viscosity.

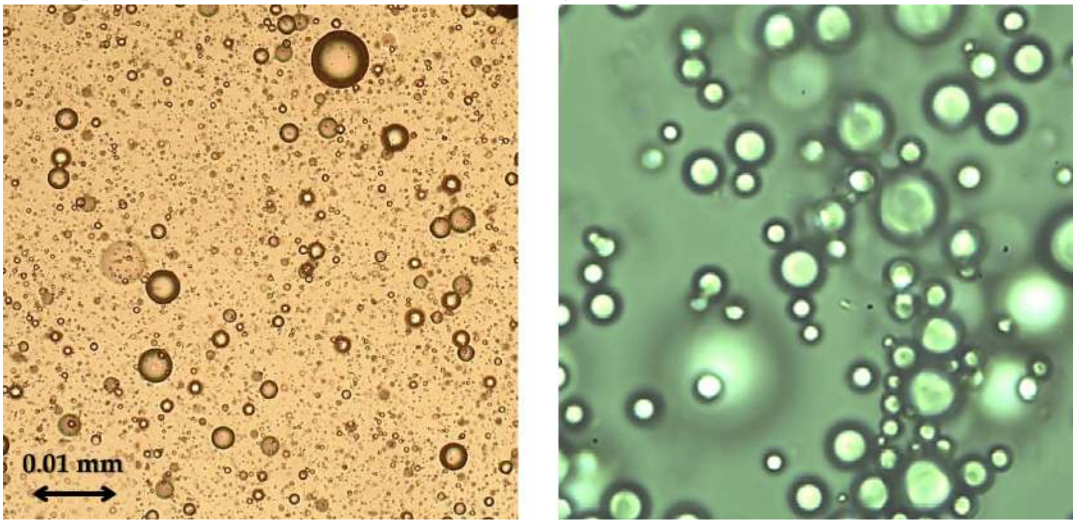

Figure 28. Water-in-oil emulsions observed with optical microscopes. Figure on the left adapted from Bulgarelli (2018). Figure on the right adapted from Valdés et al. (2020); Reproduced with permission from Chemical Engineering Science; Published by Elsevier in 2020.

For the oil-in-water emulsions, the author started with a water cut of 0%, gradually increasing to 100%, and noticed that the inversion events occurred for water fractions between 10% and 30%, approximately. To exemplify the data obtained by Bulgarelli (2018), Figure 29 contains graphics of two quantities as functions of the water fraction (w_f) and parametrized by the pump rotation speed: on the left, the dimensionless head coefficient (Ψ_m); on the right, the ratio between the emulsion (μ_e) and oil (μ_o = 55 cP) viscosities. The inversion point occurs at a w_f of 30%, in which the water-in-oil emulsion becomes an oil-in-water. Before the inversion, due to the emulsion effective viscosity with $\mu_e \geq \mu_o$, the pump performance is highly degraded and it is very similar to the condition found for a single-phase oil flow ($\Psi_{m,o}$). In contrast, after the inversion, there is a substantial reduction of μ_e with a consequent increase in the pump head, as if the device were working with single-phase water flow ($\Psi_{m,w}$). Nevertheless, it is important to emphasize that these observations are valid only for unstable emulsions, which behave differently from the stable ones.

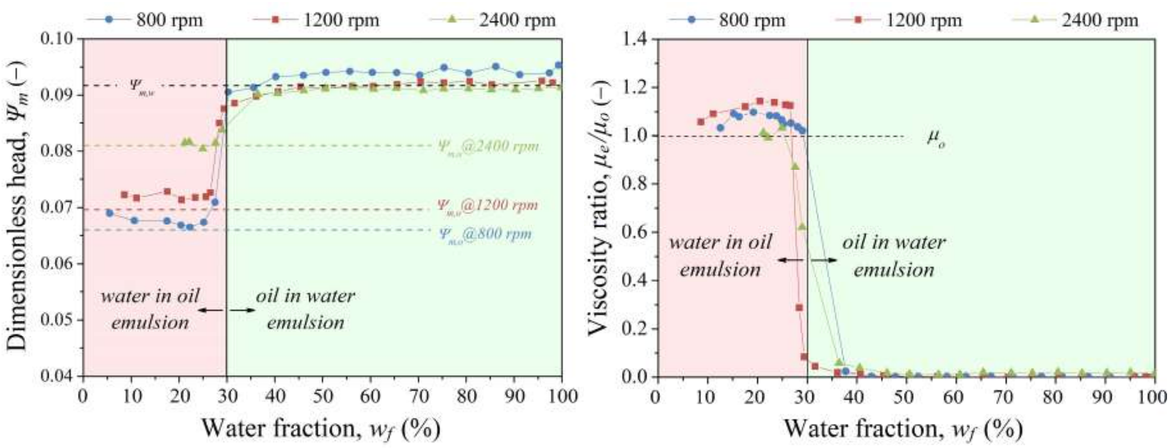

Figure 29. Quantitative analyses on phase inversion and effective viscosity for unstable emulsions in a real 8-stage ESP pump. When the water fraction (w_f) reaches approximately 30%, the dimensionless

head (Ψ_m) increases because the emulsion viscosity (μ_e) suddenly decreases. Ψ_m is proportional to H, the pump head, defined in Section 2. Figure adapted from Bulgarelli (2018).

The results achieved by Bulgarelli (2018) were extended and further interpreted in the studies by Bulgarelli et al. (2020a, 2020b). The comparison between experimental data and models for pipes indicated that there are no suitable models to predict phase inversion points in centrifugal pumps used in ESP systems. Nevertheless, the analysis of the effective viscosity was finally deepened with the use of a model proposed by Biazussi (2014) years before.

It is clear that the analysis made with OM and FBRM was important to the results obtained by Bulgarelli et al. (2020a, 2020b). As explained above, these techniques are suitable for identifying the shape and measuring the size of populations of dispersed drops, in regions outside the pump. Such methods, however, are not able to characterize the behavior and motion of individual drops, a type of information which is fundamental to the development and improvement of mathematical models. In this context, to complete their results, Bulgarelli et al. (2020b) made use of data from Perissinotto (2018), who adopted *High-Speed Imaging* to fully visualize water-oil dispersions within a pump and *Particle Tracking Velocimetry* to understand the kinematics and dynamics of single drops influenced by the impeller rotation.

The master's dissertation by Perissinotto (2018) was dedicated to study the behavior and motion of drops dispersed in the channels of a centrifugal pump impeller. To carry out his experiments, the author modified and used the pump prototype originally developed by Monte Verde (2016), whose research was reported in Section 4.2.1 above. A HSI technique together with a PTV procedure made it possible to visualize the flow and track drops in the impeller. The kinematics and dynamics of oil drops dispersed in water, with the evaluation of geometric shapes, characteristic sizes, trajectories, velocities, accelerations and main forces, were further investigated in the paper by Perissinotto et al. (2019a). Afterwards, numerical simulations that estimated velocities, forces, pressure gradients, and dissipation rates of turbulent kinetic energy were presented in the manuscript by Perissinotto et al. (2019b), in which experimental data were compared to *Computational Fluid Dynamics* results. Finally, a paper by Perissinotto et al. (2020) was published containing an analysis on the inverted dispersion, composed of samples of water drops dispersed in oil.

In all tests, the dispersed phase concentration was below 1.5% by volume. The rotational speeds varied between 300 and 1500 rpm while the continuous phase flow rates ranged between 1.0 and 6.0 m^3/h, approximately. The water-in-oil dispersion was composed of water drops in oil with viscosity of 20 cP, while the oil-in-water dispersion was composed of oil drops with 220 cP in water. In both dispersions, a dark dye was added to the dispersed phase in order to increase the contrast between the impeller hub (white) and the observed drops (black), as illustrated in Figure 30.

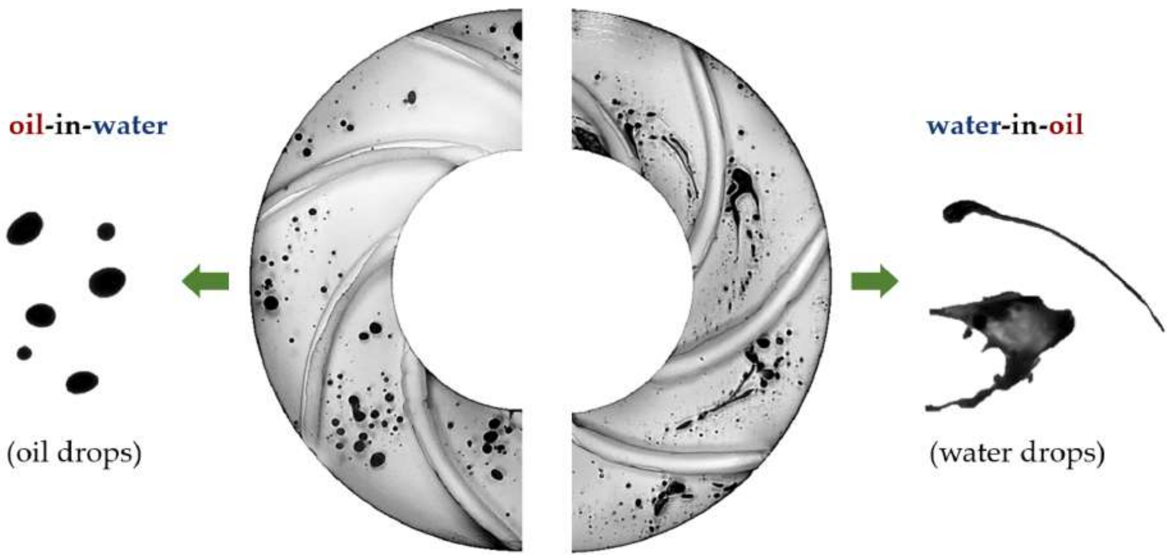

Figure 30. Two-phase liquid-liquid dispersions in the impeller of a transparent prototype rotating at 600 rpm. The continuous phase is transparent and the dispersed phase is darkened with a black dye.

The flow was visualized with HSI while the motion of liquid drops was analyzed with PTV method. Figure adapted from Perissinotto (2018).

Among the most relevant observations performed by Perissinotto (2018) and Perissinotto et al. (2019a, 2019b, 2020), the following ones stand out:

- The geometric shape and characteristic size of both oil and water drops depend directly on the fluid properties and flow conditions. An increase in the rotation speed and flow rate promotes the deformation and breakup of the dispersed drops, with a consequent reduction in their size. In addition, water drops have a greater tendency to fragment than oil drops, by reason of a low water viscosity associated with a low interfacial tension between water and mineral oil.
- The oil drops exhibit an elliptical shape with a well-defined interface, and their fragmentation is caused by turbulence in the continuous water phase which has a high Reynolds number. On the other hand, the water drops present an irregular shape with an easily deformable interface, and their breakup occurs due to shear stress which is proportional to the viscosity of the continuous oil phase. Coalescence events were not observed in any of the tests executed.
- The drops generally perform random trajectories in the impeller channels, with residence times in the order of milliseconds. The drop velocity remains around the units of meters per second, while its acceleration reaches high values in the order of hundreds of m/s^2 due to the intense centrifugal forces produced by the impeller rotating motion. The studied impeller has internal and external radii of 22 and 55 mm, respectively.
- The analysis of the drop dynamics with CFD revealed that the force due to pressure gradients is dominant over the drag force, with a difference of about one order of magnitude. Besides, the numerical simulation of trajectories indicated that the small drops follow the continuous phase streamlines, while the large drops tend to deviate from the suction towards the pressure blade by consequence of a pressure gradient formed inside the channel.

The liquid drops investigated by Perissinotto (2018) had diameters in the range from 0.1 to 6.0 millimeters. Due to limitations in the spatial resolution of high-speed cameras, it was impossible to detect drops with diameters in the order of micrometers. Therefore, the smallest drops visualized by Perissinotto (2018) with HSI were still bigger than the largest drops visualized by Bulgarelli (2018) with OM. This fact poses a challenge for both authors: connecting the results found for large drops in dispersions with the results found for small drops in emulsions.

It is true that the increase in viscosity is caused mainly by the smallest drops in the emulsions. However, according to Perissinotto et al. (2019a, 2019b, 2020), many results can be extrapolated from large to small drops, from dispersions to emulsions. For example, the forces that govern the behavior and motion of a large drop are the same as those that act on a small droplet. Drag, lift, forces due to pressure gradients, and effects caused by centrifugal and Coriolis accelerations are the same for each drop, although their intensity is usually proportional to its diameter.

Crowe et al. (2012) classify such forces as *fluid-particle interactions*, which are basically the effect of the continuous phase on the dispersed phase. These interactions would be the most relevant to the behavior and motion of dispersed drops in centrifugal pumps. However, the concentration of drops should be eventually considered in the *particle-particle interactions*, which are different for emulsions (many small drops, close to each other) and dispersions (a few large drops, away from each other). The influence of solid walls finally receives the *particle-wall interactions* designation, which may vary as a function of the place where the drop is: inside the impeller (HSI); in line but outside the pump (FBRM); or out of the experimental apparatus (OM).

The studies reviewed throughout this section are summarized in Table 4 below. As this article is interested on flow visualization, Table 4 reports studies which used devices and techniques directly or indirectly related to flow visualization in two-phase liquid-liquid flow: LPSA, UES, OMOP, EMP, OM, as well as HSI and PTV, the last ones described in Section 3.1.

Table 4. Summary of studies reviewed on the visualization of two-phase liquid-liquid flows.

Authors	Methods	Two-phase liquid-liquid flow	Pump type	Operational parameters varied	Main results achieved and parameters investigated
Ibrahim and Maloka (2006)	LPSA.	Oil-in-water emulsion without surfactant.	Radial centrifugal.	Liquid fraction, liquid flow rate, rotational speed.	Characteristic size distribution of liquid drops. Model for estimating drop diameters inside the pump.
Khalil et al. (2006, 2008)	LPSA.	Oil-in-water emulsion. Mineral oil with and without surfactant (stable and unstable).	Radial centrifugal.	Liquid fraction, liquid flow rate, rotational speed.	Emulsion viscosity. Pump performance (head, power, efficiency) in operation with the presence of emulsions.
Morales et al. (2012)	UES.	Oil-in-water emulsion. Mineral oil without surfactant addition.	Radial centrifugal.	Liquid fraction, liquid flow rate, rotational speed.	Characteristic size distribution of liquid drops. Model for estimating drop diameters. Pump performance.
Schäfer et al. (2019) and Schmitt et al. (2021)	OMOP, EMP.	Oil-in-water dispersion. Paraffin oil without surfactant addition.	Transparent replicas of centrifugal pumps.	Liquid fraction, liquid flow rate, rotational speed, impeller diameter.	Characteristic size distribution of liquid drops. Mean diameter. Energy dissipation rate.
Valdés et al. (2020)	LPSA, OM.	Oil-in-water and water-in-oil emulsion. Sunflower oil without surfactant addition.	Real ESP (4 stages).	Liquid fraction, liquid flow rate.	Emulsion rheology and morphology. Characteristic size distribution of liquid drops. Pump performance. Phase inversion points.
Bulgarelli (2018) and Bulgarelli et al. (2020a, 2020b)	LPSA, OM.	Oil-in-water and water-in-oil emulsion. Two mineral oils without surfactant.	Real ESP (8 stages).	Liquid fraction, liquid flow rate, rotational speed, oil temperature.	Phase inversion points. Calculation of effective viscosity and comparison with model. Characteristic size distribution of liquid drops. Pump performance.
Perissinotto (2018) and Perissinotto et al. (2019a, 2019b, 2020)	HSI, PTV.	Oil-in-water and water-in-oil dispersion. Two mineral oils without surfactant.	Transparent prototype based on real ESP.	Liquid fraction, liquid flow rate, rotational speed.	Study of dispersed drops: geometry; trajectory, kinematics and dynamics; breaking and coalescence; diameter distribution; numerical simulations.

From the information exposed in this section, it is possible to observe that the investigation of two-phase liquid-liquid flows inside centrifugal pumps is limited to few studies, all published in the last twenty years. Most of these studies aim to analyze the performance of pumps in operation with the presence of dispersions composed of water and oil. The characterization of such dispersions is carried out with laser (LPSA) and ultrasound (UES) analyzers, optical probes with cameras (OMOP, EMP) or microscopes (OM), which do not have direct relation to the visualization methods described in Section 3.1. These methods are suitable for measuring the size of small drops in emulsions, but they are not appropriate for the analysis of the drop dynamics within pump impellers.

Under this circumstance, the literature indicates that Perissinotto et al. (2019a, 2019b, 2020) were the first authors to use high-speed cameras (HSI, PTV) for visualization of liquid-liquid mixtures in pump impellers with focus on the behavior and motion of dispersed drops. As explained in Section 4.2.1, HSI and PTV methods are frequently applied for gas-liquid flows, but sometimes they are not adequate for liquid-liquid flows, especially when the mixture is composed by emulsions with small and concentrated drops.

5. Conclusions

In this paper, several experimental studies on flow visualization within centrifugal pumps have been reviewed in detail. Basic concepts of *Electrical Submersible Pumping* systems were presented and the most relevant flow visualization methods were described, such as *High-Speed Imaging*, *Particle Tracking Velocimetry*, *Laser-Doppler Velocimetry*, *Particle Image Velocimetry*, *Computed Tomography*, and *Optical Microscopy*. This paper provided a wide review of the state-of-the-art on the visualization of single- and two-phase flows in pump impellers.

The studies reported in this paper highlighted the preference of researchers for LDV and PIV to quantitatively investigate single-phase flows in impellers. Two-dimensional PIV is actually the most frequent. It is considered an accessible, efficient, and powerful technique that provides reliable data on the flow behavior. PIV is able to estimate velocity, vorticity, and turbulent energy, and also detect flow phenomena such as the formation of vortices and recirculation zones. The main variations of 2D-2C and 2D-3C PIV (e.g. LIF-PIV, RIM-PIV, TR-PIV) are often employed in centrifugal pumps in order to increase the temporal resolution and reduce distortions in the laser sheet. Different authors claim that these practices substantially improve the quality of the results achieved with PIV.

Regarding two-phase flows, the studies reviewed in this paper featured that HSI is the method commonly selected to identify gas-liquid flow patterns in impellers. As high-speed cameras are able to visualize fast transient phenomena with high spatial and temporal resolutions, they are regularly used to detect gas bubbles and correlate their characteristics to the pump performance. In addition, PTV is often adopted to analyze the motion of bubbles in rotating impellers, with the possibility of measuring their velocities and other derived quantities. Diversely, a few authors sometimes choose CT to obtain gas fractions in real pumps with metallic housings, as this technique does not demand the development of transparent pump prototypes. The method, which makes use of gamma-ray and x-ray radiation, has a very limited ability to identify details in the flow, such as gas-liquid interfaces, breakup and coalescence events, etc.

To a lesser extent, the HSI and PTV techniques are also used in two-phase liquid-liquid flows to investigate the behavior and motion of dispersed drops, for the analysis of shapes and sizes and the evaluation of velocities and forces, for example. However, the visualization becomes more difficult as the dispersion turns into an emulsion, with much smaller drops. In this case, the spatial resolution of high-speed cameras is insufficient and an alternative is visualizing the emulsion with an *Optical Multimode Online Probe* or an *Endoscope Measuring Probe* installed at the pump inlet or outlet. Another alternative for micrometric droplets is using the *Optical Microscopy* method, in a laboratory, with the observation of fluid samples extracted from the pump. Nevertheless, other devices as *Laser Particle Size Analyzer* and *Ultrasonic Extinction Spectrometer* may be adopted, but they are not able to actually visualize the flow, being recommended only for measuring the size of particles without identifying their geometric shapes.

Table 5 summarizes the strengths and weaknesses of each visualization method.

Table 5. Pros and cons of the main visualization methods reviewed in this article.

Main Application	Method or Device	Advantages	Limitations
Single-phase flow	LDV.	Able to measure velocities with high spatial and temporal resolutions next to solid walls.	Suitable for specific regions. High computational effort when measuring large areas or volumes.
Single-phase flow	PIV.	Able to measure velocities and derived quantities in large areas or volumes.	Temporal resolution may be low. Reflection and refraction may affect laser sheet and camera sensor.
Gas-liquid, liquid-liquid	HSI.	High spatial and temporal resolutions. Able to identify details in the flow.	Suitable for two-phase flows only. Impossible to measure velocity fields.
Gas-liquid, liquid-liquid	PTV.	Able to investigate the kinematics and dynamics of particles immersed in flows.	Particles are individually tracked. Large populations required to reduce uncertainties.
Gas-liquid	CT.	Able to visualize flows in real pumps with non-transparent metallic housings.	Limited resolutions. Unable to identify small details and measure fast fluctuations.
Liquid-liquid	OMOP, EMP, OM.	Able to visualize small liquid drops in concentrated emulsions.	Impossible to make measurements directly in the pump impeller.

6. Knowledge Gaps

From the information provided in this paper, it is evident that there are knowledge gaps in the current literature. Thus, there is room for further studies on flow visualization in centrifugal pumps. The next paragraphs discuss ideas for future studies to fill the most critical gaps.

6.1. Future Studies on Single-Phase Flows

In recent years, single-phase flows have been investigated with LDV and PIV. The vast majority of the studies available in the literature are interested in studying the water flow in a single impeller channel. Thus, there is a lack of studies involving the entire impeller in presence of viscous fluids. In this framework, the following ideas are suggested for the future:

- New experiments with PIV and its variations should be performed to study single-phase flows. The TR-PIV technique should be adopted to enable testing at higher rotational speeds, closer to the nominal speeds of real ESP systems used in the industry. Besides, it is recommended that new studies use post-processing techniques that decompose the flow according to its energetic modes. One example suitable for turbulent flows is the *Proper Orthogonal Decomposition* (POD) (Cazemier et al., 1998; Glegg and Devenport, 2001; Ben Chiekh et al., 2013), which can point out which flow structures are most related to performance losses observed in ESP impellers.
- The influence of fluid viscosity on the pump performance should be further explored with flow visualization methods. Transparent mineral oils could be used as working fluids in experiments to investigate the characteristics of viscous flows in impellers. To fill this knowledge gap, PIV seems to be the most convenient technique for identifying structures and measuring variables related to viscous flows: velocity fields, shear stresses, among others. Such information would be very useful to complement studies on the performance of pumps operating with viscous single-phase flows (e.g. Monte Verde, 2016), validate numerical simulations, or even propose and improve phenomenological models for use in the petroleum industry.
- The study of the flow in the diffuser has room to be expanded. Different techniques could be used together. Merging different PIV methods, one for the diffuser and other for the impeller, would be a solution to understand the behavior of the single-phase flow throughout the pump. The measurements could serve as a basis for modeling viscous losses in diffusers and therefore complement results normally focused on impellers.

In all cases, it is a priority that the pump prototypes are designed to enable the simultaneous visualization of all the impeller channels rather than limited regions of interest.

6.2. Future Studies on Two-Phase Gas-Liquid Flows

Gas-liquid flows are typically analyzed with HSI and PTV. These methods make it possible to measure the size of gas bubbles and also to track them to characterize their kinematics and dynamics in the impeller. On the other hand, the use of CT is still quite limited, as the method has insufficient resolution to identify small details in the flow. In this context, the following ideas are suggested as future studies:

- One of the gaps in the literature is the understanding about the effect of the number of stages on the ESP performance. The increase in pressure and shear along the stages causes the pump to tolerate more gas before experiencing surging or gas locking conditions. The study of this topic should be linked to visualization experiments, since the HSI and PTV methods could be useful to verify the relationship between the number of ESP stages and the bubble breakage rate, as well as to propose new models for bubble size distribution in the stages. To achieve the results, it would be necessary to design and build transparent pump prototypes with several impellers and diffusers. It would be a challenging task for researchers, since so far there have only been studies using prototypes with 1 to 3 stages.

- The two-phase gas-liquid flow in the pump intake is another issue that still represents a serious problem for the oil and gas sector. Few authors (e.g. Pontes, 2019) have devoted themselves to visualizing the flow in the intake region. Therefore, the use of HSI and PTV is recommended to improve the understanding on the flow patterns that occur in the intake, as well as to evaluate the relationship between pump performance and bubble size in this region.
- The study of gas bubbles, i.e. breakage rates, shapes, and sizes, should be extended to different types of pumps. As most publications are focused on radial pumps, it would be interesting to apply visualization methods in axial and mixed pumps more frequently, with analyses directed not only at the impeller, but also at the diffuser or volute. This type of research would enrich the literature.

6.3. Future Studies on Two-Phase Liquid-Liquid Flows

According to the literature, emulsions are generally analyzed with equipment based on laser or ultrasound, e.g., LPSA and UES. These devices measure the size distribution of very small drops, but they cannot actually visualize the drops to identify their shapes. Thus, an alternative is to use optical probes with cameras, e.g. OMOP and EMP, at the pump inlet or outlet. Another interesting option is to use a microscope, within the scope of OM, but it only works for mixture samples which must be extracted from the pump and analyzed outside the pump. Therefore, the visualization of emulsions *in situ* is an issue that depends on the development of techniques currently available or the creation of novel visualization devices.

In the case of dispersions whose drops have larger diameters, it is possible to visualize the flow completely with HSI and PTV methods, as it is normally done in the gas-liquid case. However, until now, few authors have dedicated themselves to the study of liquid-liquid flows using HSI and PTV. Even so, these techniques have proven to be useful for visualizing and characterizing the kinematics and dynamics of liquid drops in impellers. Studies of this nature should be expanded in the future:

- New experiments should be performed with HSI and PTV to complement current studies. The behavior and motion of dispersed drops should be analyzed at higher rotational speeds, closer to the nominal speeds of real ESP systems used in the industry. Another suggestion is to use a device for controlling the size of the drops injected in the pump. In addition, the tests should be extended to different water and oil fractions, although there is a great difficulty in visualizing flows with high dispersed phase fractions. In this case, a possible solution would be to improve data analysis using more complex techniques for image processing, based on machine learning, for example. These improvements would provide a more complete database on the two-phase liquid-liquid flows in pump impellers.
- An important knowledge gap related to the petroleum industry is the comprehension about the physical phenomena that affect the ESP behavior when it handles liquid-liquid dispersions. The implementation of PIV techniques, hence, would be a great strategy to understand the influence of dispersed phase (drops) on continuous phase (medium), and vice-versa. This type of study would provide relevant information which could be useful for proposing mathematical models to predict the pressure increment in pumps or represent the dynamics of drops dispersed in impellers. In this case, it is essential to use practices such as LIF-PIV and RIM-PIV to reduce the reflection and refraction of the laser sheet at fluid interfaces. It is also desirable to keep the fluid transparent, by avoiding the formation of emulsions, in order to be sure that the tracer particles are detected in the flow images. As an example, a possible two-phase liquid-liquid experiment could have, as working fluids, glycerin drops dispersed in mineral oil, both injected in an ESP prototype made of acrylic. Mineral oil, glycerin, and acrylic have the same refractive index, so the laser distortion in the impeller would be minimized.

7. Nomenclature List

Abbreviations	
BEP	Best Efficiency Point

CCD	Charge Coupled Device
CFD	Computational Fluid Dynamics
CMOS	Complementary Metal Oxide Semiconductor
CT	Computed Tomography
EMP	Endoscope Measuring Probe
ESP	Electrical Submersible Pump
FBRM	Focused Beam Reflectance Measurement
FFT	Fast Fourier Transform
HSI	High-Speed Imaging
LDV	Laser-Doppler Velocimetry
LPSA	Laser Particle Size Analyzer
OM	Optical Microscopy
OMOP	Optical Multimode Online Probe
POD	Proper Orthogonal Decomposition
PIV	Particle Image Velocimetry
LIF-PIV	Laser-Induced Fluorescence PIV
RIM-PIV	Refractive Index Matching PIV
TR-PIV	Time-Resolved PIV
PTV	Particle Tracking Velocimetry
UES	Ultrasonic Extinction Spectrometer

Latin Symbols	
$\boldsymbol{a}$	Fluid acceleration vector (m/s^2)
d_p	Particle diameter (m)
Δf	Frequency variation (Hz)
g	Gravity (m/s^2)
H	Pump head (m)
p	Pressure (Pa)
Δp	Pressure increment (Pa)
P_h	Hydraulic power (W)
BHP	Brake horsepower (W)
Q	Flow rate (m^3/s)
T	Torque (N.m)
t	Time instant (s)
Δt	Time interval (s)
$\boldsymbol{U}$	Fluid velocity vector (m/s)
$\boldsymbol{U_p}$	Particle velocity vector (m/s)
V	Average fluid velocity (m/s)
$\boldsymbol{X}$	Position vector of a group of particles (m)
$\boldsymbol{X_p}$	Position vector of a single particle (m)
$\Delta\boldsymbol{X}$	Displacement vector of a group of particles (m)
$\Delta\boldsymbol{X_p}$	Displacement vector of a single particle (m)
z	Vertical elevation (m)

Greek Symbols	
η	Pump efficiency (-)
θ	Angle of inclination (rad)
λ	Wavelength (m)
μ	Fluid viscosity (Pa.s)
ρ	Fluid density (kg/m^3)
ρ_p	Particle density (kg/m^3)
ω	Shaft angular velocity (rad/s)

Author Contributions: Conceptualization: Rodolfo M. Perissinotto and William Monte Verde; original draft preparation: Rodolfo M. Perissinotto and Willian D. P. Fonseca; review and editing: Rodolfo M. Perissinotto, William Monte Verde, Jorge L. Biazussi, Natan A. V. Bulgarelli; supervision: Marcelo S. de Castro and Erick de M. Franklin; project administration: Jorge L. Biazussi; funding acquisition: Antonio C. Bannwart. All authors have read and agreed to the published version of the manuscript.

Funding: This research was sponsored by Equinor Brazil and the São Paulo Research Foundation (FAPESP) in São Paulo, Brazil. The grant number is 2017/15736-3.

Acknowledgments: We gratefully acknowledge the support of EPIC – Energy Production Innovation Center, hosted by the University of Campinas (UNICAMP) and sponsored by Equinor Brazil and FAPESP. We also acknowledge the support of ANP (Brazil's National Oil, Natural Gas, and Biofuels Agency) through the R&D levy regulation. Acknowledgements are extended to the Center for Petroleum Studies (CEPETRO) and School of Mechanical Engineering (FEM) of the University of Campinas (UNICAMP), Brazil.

Conflicts of Interest: The authors declare no conflict of interest. The funders had no role in the design of the study; in the collection, analyses, or interpretation of data; in the writing of the manuscript, or in the decision to publish the results.

References

1. Abrantes, J.K.; Paula, I.B.; Azevedo, L.F.A. Medição de Escoamentos Turbulentos Utilizando Velocimetria por Imagem de Partículas. In: *Turbulência*; Carmo, B.S., Assi, G.R.S., Meneghini, J.R., Aranha, J.A.P., Volpe, E.V., Eds.; ABCM: Sao Paulo, Brazil, 2012.
2. Adrian, R.; Westerweel, J. *Particle Image Velocimetry*; Cambridge University Press: New York, USA, 2011.
3. Adrian, R.J. Twenty years of particle image velocimetry. *Exp Fluids* **2005**, *39*, pp. 159–169. doi: 10.1007/s00348-005-0991-7
4. Ahmed, T. *Reservoir Engineering Handbook*, 5th ed.; Gulf Professional Publishing: Oxford, UK, 2018.
5. Akin, O.; Rockwell, D. Flow structure in a radial flow pumping system using high-image-density particle image velocimetry. *J. Fluids Eng.* **1994**, *116*, pp. 538–544. doi: 10.1115/1.2910310
6. Al-Fatlawi, O.F.; Al-Jawad, M.; Alwan, K.A.; Essa, A.A.; Sadeq, D.; Mousa, A.J. Feasibility of gas lift to increase oil production in an Iraqi giant oil field. SPE North Africa Technical Conference and Exhibition, Cairo, Egypt, September 14-16, 2015.
7. Al-Juboori, M.; Hossain, M.; Al-Fatlawi, O.; Kabir, A.; Radhi, A. Numerical simulation of gas lift optimization using genetic algorithm for a middle east oil field: feasibility study. International Petroleum Technology Conference, Dhahran, Saudi Arabia, January 13-15, 2020.
8. Arirachakaran, S.; Oglesby, K.D.; Malinowsky, M.S.; Shoham, O.; Brill, J.P. An analysis of oil/water flow phenomena in horizontal pipes. SPE Production & Operations Symposium, Oklahoma City, USA, March 13-14, 1989.
9. Banjar, H.; Zhang, H.Q. Experiments and emulsion rheology modeling in an electric submersible pump. Proceedings of the International Petroleum Technology Conference, Beijing, China, March 26-28 2019.
10. Banjar, H.M. Experiments, CFD simulation and modeling of oil viscosity and emulsion effects on ESP performance. PhD thesis, University of Tulsa, Tulsa, USA, 2018.
11. Barrios, L.; Prado, M.G. Experimental visualization of two-phase flow inside an electrical submersible pump stage. *J. Energy Resour. Technol.* **2011a**, *133*, 042901. doi: 10.1115/1.4004966
12. Barrios, L.; Prado, M.G. Modeling two-phase flow inside an electrical submersible pump stage. *J. Energy Resour. Technol.* **2011b**, *133*, 042902. doi: 10.1115/1.4004967
13. Barrios, L.J. Visualization and modeling of multiphase performance inside an electrical submersible pump. PhD thesis, University of Tulsa, Tulsa, USA, 2007.
14. Ben Chiekh, M.; Michard, M.; Guellouz, M.S.; Béra, J.C. POD analysis of momentumless trailing edge wake using synthetic jet actuation. *Exp. Therm. Fluid Sci.* **2013**, *46*, pp. 89–102. doi: 10.1016/j.expthermflusci.2012.11.024

15. Biazussi, J.L. A drift-flux model for gas-liquid flow in electrical submersible pump operating with low viscous liquid. PhD thesis, University of Campinas, Campinas, Brazil, 2014.

16. Bieberle, A.; Schleicher, E.; Hampel, U. Data acquisition system for angle synchronized γ-ray tomography of rapidly rotating objects. *Meas. Sci. Technol*. **2007**, *18*, pp. 3384–3390. doi: 10.1088/0957-0233/18/11/018

17. Boutier, A. *Laser Velocimetry in Fluid Mechanics*; John Wiley & Sons: New York, USA, 2013.

18. Bracewell, R. N. *The Fourier Transform and its Applications*, 3rd ed.; McGraw-Hill: New York, USA, 1999.

19. Brauner, N.; Ullmann, A. Modeling of phase inversion phenomenon in two-phase pipe flows. *Int. J. Multiphas. Flow* **2002**, *28*, pp. 1177–1204. doi: 10.1016/S0301-9322(02)00017-4

20. Bremner, C.; Harris, G.; Kosmala, A.; Nicholson, B.; Ollre, A.; Pearcy, M.; Salmas, C.J.; Solanki, S.C. Evolving technologies: electrical submersible pumps. *Oilfield Review* **2006**, pp. 30–43.

21. Brennen, C.E. *Hydrodynamics of Pumps*; Cambridge University Press: New York, USA, 2011.

22. Brinkman, H.C. The viscosity of concentrated suspensions and solutions. *J. Phys. Chem*. **1952**, *20*, pp. 571. doi: 10.1063/1.1700493

23. Brossard, C.; Monnier, J.C.; Barricau, P.; Vandernoot, F.X.; Le Sant, Y.; Champagnat, F.; Le Besnerais, G. Principles and applications of particle image velocimetry. *Onera Aerospacelab Journal* **2009**, *1.*

24. Buchhave, P. Particle image velocimetry - status and trends. *Exp. Therm. Fluid Sci.* **1992**, *5*, pp. 586–604. doi: 10.1016/0894-1777(92)90016-X

25. Budwig, R. Refractive index matching methods for liquid flow investigations. *Exp. Fluids* **1994**, *17*, pp. 350–355. doi: 10.1007/BF01874416

26. Bulgarelli, N.A.V. Experimental study of electrical submersible pump (ESP) operating with water/oil emulsion. MSc dissertation, University of Campinas, Campinas, Brazil, 2018.

27. Bulgarelli, N.A.V.; Biazussi, J.L.; Monte Verde, W.; Castro, M.S.; Bannwart, A.C. Experimental study of phase inversion phenomena in electrical submersible pumps under oil/water flow. *J. Offshore Mech. Arct. Eng.* **2020a**, *142*, 041402. doi: 10.1115/1.4045787

28. Bulgarelli, N.A.V.; Biazussi, J.L.; Monte Verde, W.; Perles, C.E.; Castro, M.S.; Bannwart, A.C. Experimental investigation on the performance of electrical submersible pump (ESP) operating with unstable water/oil emulsions. *J. Petrol. Sci. Eng.* **2020b**, *197*, 107900. doi: 10.1016/j.petrol.2020.107900

29. Byskov, R.K.; Jacobsen, C.B.; Pedersen, N. Flow in a centrifugal pump impeller at design and off-design conditions - Part I: large eddy simulations. *J. Fluids Eng.* **2003**, *125*, pp. 73–83. doi: 10.1115/1.1524586

30. Carneiro, J.N.E.; Patil, A.; Johansen, S.T.; Gonçalves, G.F.N.; Gallassi, M. Drop Breakup and Size Evolution in Oil and Gas Production: A Review of Models and Mechanisms. In: *Droplet and Spray Transport: Paradigms and Applications*; Basu, S., Agarwal, A.K., Mukhopadhyay, A.; Patel, C., Eds.; Springer Nature Singapore: Singapore, 2018. doi: 10.1007/978-981-10-7233-8_5

31. Castro, M.S.; Rodriguez, O.M.H. Interfacial waves in stratified viscous oil–water flow. *Exp. Therm. Fluid Sci.* **2015**, *62*, pp. 85–98. doi: 10.1016/j.expthermflusci.2014.12.003

32. Cavazzini, G.; Pavesi, G.; Ardizzon, G. Analysis of the rotor-stator interaction in a radial flow pump. *La Houille Blanche* **2009**, *5*, pp. 141–151. doi: 10.1051/lhb/2009067

33. Cavicchio, C.A.M.; Biazussi, J.L.; Castro, M.S.; Bannwart, A.C.; Rodriguez, O.M.H.; Carvalho, C.H.M. Experimental study of viscosity effects on heavy crude oil-water core-annular flow pattern. *Exp. Therm. Fluid Sci.* **2018**, *92*, pp. 270–285. doi: 10.1016/j.expthermflusci.2017.11.027

34. Cazemier, W.; Verstappen, R.W.C.P; Veldman, A.E.P. Proper orthogonal decomposition and low-dimensional models for driven cavity flows. *Phys. Fluids* **1998**, *10*. doi: 10.1063/1.869686

35. Cortes, B.; Araujo, L.R.; Penido, D.R. Electrical submersible pump system model to assist oil lifting studies. *J. Petrol. Sci. Eng.* **2019**, *174*, pp. 1279-1289. doi: 10.1016/j.petrol.2018.11.055

36. Cressler, J.D. Silicon Earth: Introduction to the Microelectronics and Nanotechnology Revolution, 2nd ed.; CRC Press: Boca Raton, USA, 2016.

37. Croce, D.; Pereyra, E. Study of oil/water flow and emulsion formation in electrical submersible pumps. *SPE Production & Operations* **2020**, 35, pp. 26–36. doi: 10.2118/198900-PA
38. Crowe, C.T.; Schwarzkopf, J.D.; Sommerfeld, M.; Tsuji, Y. *Multiphase Flows with Droplets and Particles*, 2nd ed.; CRC Press: Boca Raton, USA, 2012.
39. Cubas, J.M.C.; Stel, H.; Ofuchi, E.M.; Neto, M.A.M.; Morales, R.E.M. Visualization of two-phase gas-liquid flow in a radial centrifugal pump with a vaned diffuser. *J. Petrol. Sci. Eng.* **2020**, *187*, 106848. doi: 10.1016/j.petrol.2019.106848
40. Dong, R.; Chu, S.; Katz, J. Quantitative visualization of the flow within the volute of a centrifugal pump. Part A: technique. *J. Fluids Eng.* **1992a**, *114*, pp. 390–395. doi: 10.1115/1.2910043
41. Dong, R.; Chu, S.; Katz, J. Quantitative visualization of the flow within the volute of a centrifugal pump. Part B: results and analysis. *J. Fluids Eng.* **1992b**, *114*, pp. 396–403. doi: 10.1115/1.2910044
42. Dracos, T. Particle Tracking Velocimetry (PTV). In: *Three-Dimensional Velocity and Vorticity Measuring and Image Analysis Techniques*; Dracos, T., Ed.; Springer: Dordrecht, Germany, 1996.
43. Duplaa, S.; Coutier-Delgosha, O.; Dazin, A.; Bois, G. X-ray measurements in a cavitating centrifugal pump during fast start-ups. *J. Fluids Eng.* **2013**, *135*, 041204. doi: 10.1115/1.4023677
44. Einstein, A. Berichtigung zu meiner arbeit: "Eine neue bestimmung der moleküldimensionen". *Annalen der Physik* **1911**, *339*, pp. 591–592. doi: 10.1002/andp.19113390313
45. Einstein, A. Eine neue bestimmung der moleküldimensionen. *Annalen der Physik* **1906**, *324*, pp. 289–306. doi: 10.1002/andp.19063240204
46. Equinor. Energy Perspectives: long-term macro and market outlook. 2019, pp. 36.
47. Estevam, V. Phenomenological analysis about centrifugal pump in two-phase flow operation. PhD thesis, University of Campinas, Campinas, Brazil, 2002.
48. Feng, J.; Benra, F.K.; Dohmen, H.J. Comparison of periodic flow fields in a radial pump among CFD, PIV, and LDV results. *Int. J. Rotating Mach.* **2009**, *2009*, 410838. doi: 10.1155/2009/410838
49. Flatern, R. The Defining Series: Electrical Submersible Pumps. *Oilfield Review* **2015**, pp. 1–2.
50. Fox, R.W.; Pritchard, P.J.; McDonald, A.T. *Introdução à Mecânica dos Fluidos*, 7th ed.; LTC: Rio de Janeiro, Brazil, 2011; pp. 433–513.
51. Freymuth, P. Flow visualization in fluid mechanics. *Rev. Sci. Instrum.* **1993**, *64*. doi: 10.1063/1.1144433
52. Gamboa, J.; Prado, M.G. Visualization study of performance breakdown in two-phase performance of an electrical submersible pump. Proceedings of the 26th Int Pump Users Symposium, Houston, USA, 2010.
53. Gerlach, A. The influence of impeller designs on the performance of a vortex pump. MSc dissertation, Technical University of Berlin, Berlin, Germany, 2018.
54. Gharib, M.; Kremers, D.; Koochesfahani, M.M.; Kemp, M. Leonardo's vision of flow visualization. *Exp. Fluids* **2002**, *33*, pp. 219–223. doi: 10.1007/s00348-002-0478-8
55. Giordano, R.; Astarita, T. Spatial resolution of the Stereo PIV technique. *Exp. Fluids*. **2009**, *46*, pp. 643. doi: 10.1007/s00348-008-0589-y
56. Glegg, S.A.L; Devenport, W.J. Proper orthogonal decomposition of turbulent flows for aeroacoustic and hydroacoustic applications. *J Sound Vib* **2001**, *239*, pp. 767–784. doi: 10.1006/jsvi.2000.3128
57. Grant, I. Particle image velocimetry: a review. *J. Mech. Eng*. **1997**, *211*, p. 55–76. doi: 10.1243/0954406971521665
58. Guet, S.; Rodriguez, O.M.H.; Oliemans, R.V.A.; Brauner, N. An inverse dispersed multiphase flow model for liquid production rate determination. *Int. J. Multiphase Flow* **2006**, *32*, pp. 553–567. doi: 10.1016/j.ijmultiphaseflow.2006.01.008
59. Gülich, J.F. *Centrifugal Pumps*; Springer: Berlin, Germany, 2008.
60. Hartenbach, G.; Magalhães, J.; Belsvik, Y.; Pessoa, R.; Lemos, D. Well performance and production optimization through the use of ESPs as artificial lift method. SPE Artificial Lift Conference, Salvador, Brazil, May 27-28, 2015. doi: 10.2118/173972-MS

61. Hassan, W.; Legoupil, S.; Chambellan, D.; Barre, S. Dynamic localization of vapor fraction in turbo pump inducers by x-ray tomography. *IEEE Trans. Nucl. Sci.* **2008**, *55*, pp. 656–661. doi: 10.1109/TNS.2007.914023

62. Honório, W.; Lemos, D.; Lima, R. ESP control and monitoring system of heavy oil Peregrino field. SPE Artificial Lift Conference, Salvador, Brazil, May 27-28, 2015. doi: 10.2118/173929-MS

63. Hydraulic Institute Standards. Effects of Liquid Viscosity on Rotor Dynamic Pump Performance. ANSI-HI 9.6.7 - 2010.

64. Ibrahim, S.Y.; Maloka, I.E. Emulsification of secondary oil/water dispersions using a centrifugal pump. *Petrol. Sci. Technol*. **2006**, *24*, pp. 513–522. doi: 10.1081/LFT-200041121

65. Jähne, B. *Digital Image Processing*, 6th ed.; Springer: Heidelberg, Germany, 2005.

66. Keller, J. Fluid-dynamic fluctuations and flow structures in centrifugal pumps due to rotor-stator interaction. PhD thesis, University of Oviedo, Gijón, Spain, 2014.

67. Keller, J.; Blanco, E.; Barrio, R.; Parrondo, J. PIV measurements of the unsteady flow structures in a volute centrifugal pump at a high flow rate. *Exp. Fluids* **2014**, *55*, 1820. doi: 10.1007/s00348-014-1820-7

68. Khalil, M.; Kassab, S.; Ismail, A.; Elazab, I. Centrifugal pump performance under stable and unstable oil-water emulsions flow. Proceedings of the 12th Int Water Technology Conference, Alexandria, Egypt, March 27-30, 2008.

69. Khalil, M.; Kassab, S.; Ismail, A.; Elazab, I. Influence of various parameters on the characteristics of stable and unstable oil-in-water emulsion. Proceedings of the 8th International Conference of Fluid Dynamics and Propulsions, Sharm El-Sheikh, Egypt, December 2006.

70. Kokal, S.L. Crude oil emulsions: a state-of-the-art review. *SPE Production & Facilities* **2005**, *20*, SPE-77497-PA. doi: 10.2118/77497-PA

71. Krause, N.; Pap, E.; Thévenin, D. Investigation of off-design conditions in a radial pump by using time-resolved-PIV. Proceedings of the 13th Int Symp on Applications of Laser Techniques to Fluid Mechanics, Lisbon, Portugal, June 26-29, 2006.

72. Krieger, I.M. Rheology of monodisperse latices. *Adv. Colloid Interface Sci*. **1972**, *3*, pp. 111–136. doi: 10.1016/0001-8686(72)80001-0

73. Lea, J.F.; Bearden, J.L. Effect of gaseous fluids on submersible pump performance. *J. Pet. Technol.* **1982**, *34*, pp. 2922–2930. doi: 10.2118/9218-PA

74. Li, X.; Chen, B.; Luo, X.; Zhu, Z. Effects of flow pattern on hydraulic performance and energy conversion characterization in a centrifugal pump. *Renew. Energy* **2020**, *151*, pp. 475–487. doi: 10.1016/j.renene.2019.11.049

75. Lugt, H.J. *Vortex flow in nature and technology*; Wiley-Interscience: New York, USA, 1983.

76. Maas, H.G.; Gruen, A.; Papantoniou, D. Particle tracking velocimetry in three-dimensional flows. Part 1. *Exp. Fluids* **1993**, *15*, pp. 133–146. doi: 10.1007/BF00190953

77. Malik, N.A.; Dracos, T.; Papantoniou, D. Particle tracking velocimetry in three-dimensional flows. Part 2. *Exp. Fluids* **1993**, *15*, pp. 279–294. doi: 10.1007/BF00223406

78. Melling, A. Tracer particles and seeding for particle image velocimetry. *Meas. Sci. Technol.* **1997**, *8*, pp. 1406–1416. doi: 10.1088/0957-0233/8/12/005

79. Merzkirch, W. *Flow Visualization*, 2nd ed.; Academic Press: Orlando, USA, 1987.

80. Minemura, K.; Murakami, M. A theoretical study on air bubble motion in a centrifugal pump impeller. *J. Fluids Eng.* **1980**, *102*, pp. 446–453. doi: 10.1115/1.3240721

81. Mittag, S.; Gabi, M. Experimental investigation on pump-intake-elbow systems using refraction index matching and TR-SPIV. Proceedings of the Int Symp on Transport Phenomena and Dynamics of Rotating Machinery, Honolulu, Hawaii, April 10-15, 2016.

82. Mohammadi, M.; Sharp, K.V. Experimental techniques for bubble dynamics analysis in microchannels: a review. *J. Fluids Eng.* **2013**, *135*, 021202–1. doi: 10.1115/1.4023450

83. Molki, A.; Kheezar, L.; Goharzadeh, A. Measurement of fluid velocity development in laminar pipe flow using laser doppler velocimetry. *Eur. J. Phys.* **2013**, *34*, pp. 1127–1134. doi: 10.1088/0143-0807/34/5/1127

84. Monte Verde, W. Performance modeling of ESP pumps performance operating with gas-viscous liquid mixtures. PhD thesis, University of Campinas, Campinas, Brazil, 2016.

85. Monte Verde, W.; Biazussi, J.L.; Sassim, N.A.; Bannwart, A.C. Experimental study of gas-liquid two-phase flow patterns within centrifugal pumps impellers. *Exp. Therm. Fluid Sci.* **2017**, *85*, pp. 37–51. doi: 10.1016/j.expthermflusci.2017.02.019

86. Morales, R.; Pereyra, E.; Wang, S.; Shoham, O. Droplet formation through centrifugal pumps for oil-in-water dispersions. *SPE Journal* **2012**, *18*, pp. 172–178. doi: 10.2118/163055-PA

87. Murakami, M.; Minemura, K. Effects of entrained air on the performance of a centrifugal pump (1st report, performance and flow conditions). *Bulletin of Japan Society of Mechanical Engineers* **1974a**, *17*, pp. 1047–1055.

88. Murakami, M.; Minemura, K. Effects of entrained air on the performance of a centrifugal pump (2nd report, effects of number of blades). *Bulletin of Japan Society of Mechanical Engineers* **1974b**, *17*, pp. 1286–1295.

89. Nädler, M.; Mewes, D. Flow induced emulsification in the flow of two immiscible liquids in horizontal pipes. *Int. J. Multiphas. Flow* **1997**, *23*, pp. 55–68. doi: 10.1016/S0301-9322(96)00055-9

90. Nagabhushana, S.; Sathyanarayana, N. *Lasers and Optical Instrumentation*; IK International Pvt Ltd.: New Delhi, India, 2010.

91. Neumann, M.; Schäfer, T.; Bieberle, A.; Hampel, U. An experimental study on the gas entrainment in horizontally and vertically installed centrifugal pumps. *J. Fluids Eng.* **2016**, *138*, 091301. doi: 10.1115/1.4033029

92. Ngan, K.H.; Ioannou, K.; Rhyne, L.D.; Wang, W.; Angeli, P. A methodology for predicting phase inversion during liquid-liquid dispersed pipeline flow. *Chem. Eng. Res. Des.* **2009**, *87*, pp. 318–324. doi: 10.1016/j.cherd.2008.09.012

93. Paone, N.; Riethmuller, M.L.; Braembussche, R.A. Experimental investigation of the flow in the vaneless diffuser of a centrifugal pump by particle image displacement velocimetry. *Exp. Fluids* **1989**, *7*, pp. 371-378. doi: 10.1007/BF00193417

94. Paone, N.; Scalise, L.; Tomasini, E.P. Laser Doppler Velocimetry. In: *An Introduction to Optoelectronic Sensors*; Righini, G.C., Tajani, A., Cutolo, A., Eds.; World Scientific: Singapore, 2009.

95. Pavlov, A.; Sannaes, B.H. Experimental studies of ESP performance with two-phase fluids with live viscous oils. Proceedings of the World Heavy Oil Congress, Aberdeen, Scotland, September 2012.

96. Pedersen, N. Experimental investigation of flow structures in a centrifugal pump impeller using Particle Image Velocimetry. PhD thesis, Technical University of Denmark, Kongens Lyngby, Denmark, 2000.

97. Pedersen, N.; Larsen, P.S.; Jacobsen, C.B. Flow in a centrifugal pump impeller at design and off-design conditions - Part I: particle image velocimetry (PIV) and laser doppler velocimetry (LDV) measurements. *J. Fluids Eng.* **2003**, *125*, pp. 61–72. doi: 10.1115/1.1524585

98. Perissinotto, R.M. Experimental study of dispersed liquid-liquid two-phase flow within impellers of centrifugal pumps. MSc dissertation, University of Campinas, Campinas, Brazil, 2018.

99. Perissinotto, R.M.; Monte Verde, W.; Castro, M.S.; Biazussi, J.L.; Estevam, V.; Bannwart, A.C. Experimental investigation of oil drops behavior in dispersed oil-water two-phase flow within a centrifugal pump impeller. *Exp. Therm. Fluid Sci.* **2019a**, *105*, pp. 11–26. doi: 10.1016/j.expthermflusci.2019.03.009

100. Perissinotto, R.M.; Monte Verde, W.; Gallassi, M.; Gonçalves, G.F.N.; Castro, M.S.; Carneiro, J.; Biazussi, J.L.; Bannwart, A.C. Experimental and numerical study of oil drop motion within an ESP impeller. *J. Petrol. Sci. Eng.* **2019b**, *175*, pp. 881–895. doi: 10.1016/j.petrol.2019.01.025

101. Perissinotto, R.M.; Monte Verde, W.; Perles, C.E.; Biazussi, J.L.; Castro, M.S.; Bannwart, A.C. Experimental analysis on the behavior of water drops dispersed in oil within a centrifugal pump impeller. *Exp. Therm. Fluid Sci.* **2020**, *112*, 109969. doi: 10.1016/j.expthermflusci.2019.109969

102. Perissinotto, R.M.; Saturnino, J.; Monte Verde, W.; Biazussi, J.L., Castro, M.S., Bannwart, A. Experimental image analysis of gas bubble path line in centrifugal pump impeller. Proceedings of the 24th International

Congress of Mechanical Engineering (COBEM), Curitiba, Brazil, December 3-8, 2017. doi: 10.26678/ABCM.COBEM2017.COB17-0982

103. Pfleiderer, C.; Petermann, H. *Máquinas de Fluxo*. Livros Técnicos e Científicos: Rio de Janeiro, Brazil, 1979.

104. Plasencia, J.; Pettersen, B.; Nydal, O.J. Pipe flow of water-in-crude oil emulsions: Effective viscosity, inversion point and droplet size distribution. *J. Petrol. Sci. Eng.* **2013**, *101*, pp. 35–43. doi: 10.1016/j.petrol.2012.11.009

105. Poullikkas, A. Effects of two-phase liquid-gas flow on the performance of nuclear reactor cooling pumps. *Progress in Nuclear Energy* **2003**, *42*, pp. 3–10. doi: 10.1016/S0149-1970(03)80002-1

106. Raffel, M.; Willert, C.E.; Wereley, S.; Kompenhans, J. *Particle Image Velocimetry: A Practical Guide*, 2nd ed.; Springer: Berlin, Germany, 2007.

107. Renk, K.F. *Basics of Laser Physics*, 2nd ed.; Springer: Cham, Switzerland, 2017.

108. Rocha, A.D.; Bannwart, A.C.; Ganzarolli, M.M. Numerical and experimental study of an axially induced swirling pipe flow. *Int. J. Heat Fluid Fl.* **2015**, *53*, pp. 81–90. doi: 10.1016/j.ijheatfluidflow.2015.02.003

109. Rosa, A.J.; Carvalho, R.S.; Xavier, J.A.D. *Engenharia de Reservatórios de Petróleo*; Editora Interciência: Rio de Janeiro, Brazil, 2006.

110. Sato, S.; Furukawa, A.; Takamatsu, Y. Air-water two-phase flow performance of centrifugal pump impellers with various blade angles. *JSME International Journal* **1996**, *39*, pp. 223–229. doi: 10.1299/jsmeb.39.223

111. Scarano, F.; David, L.; Bsibsi, M.; Calluaud, D. S-PIV comparative assessment: image dewarping + misalignment correction and pinhole + geometric back projection. *Exp. Fluids*. **2005**, *39*, pp. 257–266. doi: 10.1007/s00348-005-1000-x

112. Scarano, F. Tomographic PIV: principles and practice. *Meas. Sci. Techol.* **2012**, *24*, 012001. doi: 10.1088/0957-0233/24/1/012001

113. Schäfer, J.; Schmitt, P.; Hlawitschka, M.W.; Bart, H.J. Measuring particle size distributions in multiphase flows using a convolutional neural network. *Chem. Ing. Tech.* **2019**, *91*, pp. 1688–1695. doi: 10.1002/cite.201900099

114. Schäfer, T.; Bieberle, A.; Neumann, M.; Hampel, U. Application of gamma-ray computed tomography for the analysis of gas holdup distributions in centrifugal pumps. *Flow Meas. Instrum.* **2015**, *46*, pp. 262–267. doi: 10.1016/j.flowmeasinst.2015.06.001

115. Schäfer, T.; Neumann -Kipping, M.; Bieberle, A.; Bieberle, M.; Hampel, U. Ultrafast x-ray computed tomography imaging for hydrodynamic investigations of gas-liquid two-phase flow in centrifugal pumps. *J. Fluids Eng.* **2020**, *142*, 041502. doi: 10.1115/1.4045497

116. Schäfer, T.; Neumann, M.; Bieberle, A.; Hampel, U. Experimental investigations on a common centrifugal pump operating under gas entrainment conditions. *Nucl. Eng. Des*. **2017**, *316*, pp. 1–8. doi: 10.1016/j.nucengdes.2017.02.035

117. Schmetterer, L.; Garhofer, G. How can blood flow be measured? *Survey of Ophthalmology* **2007**, *52*, pp. S134-S138. doi: 10.1016/j.survophthal.2007.08.008

118. Schmitt, P.; Sibirtsev, S.; Hlawitschka, M.W.; Styn, R.; Jupke, A.; Bart, H.J. Droplet size distribution of liquid-liquid dispersions in centrifugal pumps. *Chem. Ing. Tech.* **2021**, *93*. doi: 10.1002/cite.202000180

119. Schosser, C.; Fuchs, T.; Hain, R.; Kähler, C.J. Non-intrusive calibration for three-dimensional particle imaging. *Exp. Fluids.* **2016**, *57*, pp. 69. doi: 10.1007/s00348-016-2167-z

120. Shao, C.; Li, C.; Zhou, J. Experimental investigation of flow patterns and external performance of a centrifugal pump that transports gas-liquid two-phase mixtures. *Int. J. Heat Fluid Fl.* **2018**, *71*, pp. 460–469. doi: 10.1016/j.ijheatfluidflow.2018.05.011

121. Shoham, O. *Mechanistic Modeling of Gas-Liquid Two-Phase Flow in Pipes*; The Society of Petroleum Engineers (SPE): Tulsa, USA, 2006.

122. Sinha, M.; Katz, J. Quantitative visualization of the flow in a centrifugal pump with diffuser vanes: flow structures and turbulence. *J. Fluids Eng.* **2000**, *122*, pp. 97–107. doi: 10.1115/1.483231

123. Sjöblom, J. *Emulsions and Emulsion Stability*, 2nd ed.; CRC Press: Boca Raton, USA, 2005.

124. Smits, A.J.; Lim, T.T. *Flow Visualization: Techniques and Examples*, 2nd ed.; Imperial College Press: London, UK, 2012.

125. Solano, E.A. Viscous effects on the performance of electro submersible pumps (ESP's). MSc dissertation, University of Tulsa, Tulsa, USA, 2009.

126. Stel, H.; Ofuchi, E.M.; Sabino, R.H.G.; Ancajima, F.C.; Bertoldi, D.; Neto, M.A.M.; Morales, R.E.M. Investigation of the motion of bubbles in a centrifugal pump impeller. *J. Fluids Eng.* **2019**, *141*, 031203. doi: 10.1115/1.4041230

127. Stepanoff, A.J. *Centrifugal and Axial Flow Pumps*, 2nd ed.; Krieger Publishing Co.: Malabar, USA, 1957.

128. Tadros, T.F. *Emulsion Formation and Stability*; Wiley-VCH: Weinheim, Germany, 2013.

129. Takacs, G. Electrical Submersible Pumps Manual: Design, Operations, and Maintenance, 2nd ed.; Gulf Professional Publishing: Oxford, UK, 2017.

130. Thoroddsen, S.T.; Etoh, T.G.; Takehara, K. High-speed imaging of drops and bubbles. *Annu. Rev. Fluid Mech.* **2008**, *40*, pp. 257–285. doi: 10.1146/annurev.fluid.40.111406.102215

131. Thum, D.; Hellmann, D.H.; Sauer, M. Influence of the patterns of liquid-gas flows on multiphase-pumping of radial centrifugal pumps. Proceedings of the 5th North American Conf on Multiphase Technology, Banff, Canada, May 31 – June 2, 2006.

132. Trevisan, F.E.; Prado, M.G. Experimental investigation on the viscous effect on two-phase flow patterns and hydraulic performance of electrical submersible pumps. *J. Can. Petrol. Technol.* **2011**, *50*, pp. 45–52. doi: 10.2118/134089-PA

133. Trevisan, F.E.; Prado, M.G. The development and water-air two-phase test results of an electrical submersible pump visualization prototype. *WIT Transactions on Eng. Sci.* **2010**, *69*, pp. 485–496. doi: 10.2495/AFM100421

134. U.S. Energy Information Administration: Frequently Asked Questions. Available online: https://www.eia.gov/tools/faqs/faq.php?id=709&t=6 (accessed on 28 April 2020).

135. Valdés, J.P.; Asuaje, M.; Ratkovich, N. Study of an ESP's performance handling liquid-liquid flow and unstable O-W emulsions. Part I: Experimental. *Chem. Eng. Sci*. **2020**, *223*, 115726. doi: 10.1016/j.ces.2020.115726

136. van Houwelingen, J.; Holten, A.P.; Clercx, H.J.; Kunnen, R.P.; Molenaar, J.; van de Water, W. Visualizing large-scale flow using synthetic aperture PIV. *Exp. Fluids*. **2020**, *61*. doi: 10.1007/s00348-019-2836-9

137. Vand, V. Viscosity of solutions and suspensions: I. Theory. *J. Phys. Chem*. **1948**, *52*, pp. 277–299. doi: 10.1021/j150458a001

138. Vieira, S.C.; Geest, C.; Fabro, A.T.; Castro, M.S.; Bannwart, A.C. Experimental study and modelling of developing intermittent slug flow in inclined annular pipelines. *J. Petrol. Sci. Eng.* **2020**, *192*, 107204. doi: 10.1016/j.petrol.2020.107204

139. Volk, M. *Pump Characteristics and Applications*, 3rd ed.; CRC Press: Boca Raton, USA, 2013; pp. 192.

140. Wernet, M.P. Development of digital particle imaging velocimetry for use in turbomachinery. *Exp. Fluids* **2000**, *28*, pp. 97–115. doi: 10.1007/s003480050015

141. Westra, R.W.; Broersma, L.; Andel, K.; Kruyt, N.P. PIV measurements and CFD computations of secondary flow in a centrifugal pump impeller. *J. Fluids Eng.* **2010**, *132*, 061104. doi: 10.1115/1.4001803

142. White, F.M. *Fluid Mechanics*, 7th ed.; McGraw-Hill: New York, USA, 2011; pp. 759–823.

143. Wieneke, B. Stereo-PIV using self-calibration on particle images. *Exp. Fluids*. **2005**, *39*, pp. 267–280. doi: 10.1007/s00348-005-0962-z

144. Willert, C.E.; Gharib, M. Digital particle image velocimetry. *Exp. Fluids*. **1991**, *10*, pp. 181–193. doi: 10.1007/BF00190388

145. Wilson, D.G. Turbomachinery—from paddle wheels to turbojets. *Mech. Eng*. **1982**, *104*, pp. 28–40.

146. Worth, D.; Al-Safran, E.; Choudhuri, A.; Al-Jasmi, A. Assessment of artificial lift methods for a heavy oil field in Kuwait. *J. Petrol. Sci. Eng.* **2019**, *180*, pp. 835–843. doi: 10.1016/j.petrol.2019.06.012

147. Wu, Y.L.; Liu, S.H.; Yuan, H.J.; Shao, J. PIV measurement on internal instantaneous flows of a centrifugal pump. *Sci. China Technol. Sc.* **2011**, *54*, pp. 270–276. doi: 10.1007/s11431-010-4262-3

148. Wu, Y.L.; Yuan, H.J.; Shao, J.; Liu, S.H. Experimental study on internal flow of a mini centrifugal pump by PIV measurement. *Int. J. Fluid Machinery Systems*, **2009**, *2*, pp. 121–126. doi: 10.5293/IJFMS.2009.2.2.121

149. Wuibaut, G.; Bois, G.; Dupont, P.; Caignaert, G.; Stanislas, M. PIV measurements in the impeller and the vaneless diffuser of a radial flow pump in design and off-design operating conditions. *J. Fluids Eng.* **2002**, *124*, pp. 791–797. doi: 10.1115/1.1486473

150. Wulff, D.L. PIV Measurements in Pumps. In *Design and Analysis of High Speed Pumps*, Educational Notes RTO-EN-AVT-143 Paper 5. RTO: Neuilly-sur-Seine, France, 2006; pp. 5-1 – 5-36.

151. Yang, H.; Xu, H.R.; Liu, C. Flow measurements in a model centrifugal pump by 3D PIV. *IOP Conf. Ser.: Earth Environ. Sci.* **2012**, 15, 062053. doi: 10.1088/1755-1315/15/6/062053

152. Yaron, I.; Gal-Or, B. On viscous flow and effective viscosity of concentrated suspensions and emulsions. *Rheologica Acta* **1972**, *11*, pp. 241–252. doi: 10.1007/BF01974767

153. Yeh, G.C.; Haynie, F.H.; Moses, R.A. Phase-volume relationship at the point of phase inversion in liquid dispersions. *AIChE Journal* **1964**, *10*, pp. 260–265. doi: 10.1002/aic.690100224

154. Zhang, J.; Cai, S.; Li, Y.; Zhu, H.; Zhang, Y. Visualization study of gas-liquid two-phase flow patterns inside a three-stage rotodynamic multiphase pump. *Exp. Therm. Fluid Sci.* **2016**, *70*, pp. 125–138. doi: 10.1016/j.expthermflusci.2015.08.013

155. Zhao, L., Chang, Z., Zhang, Z., Huang, R., He, D. Visualization of gas-liquid flow pattern in a centrifugal pump impeller and its influence on the pump performance. *Measurement: Sensors* **2021**, 13, 100033. doi: 10.1016/j.measen.2020.100033

156. Zhu, J.; Zhang, H.Q. A review of experiments and modeling of gas-liquid flow in electrical submersible pumps. *Energies* **2018**, *11*. doi: 10.3390/en11010180

157. Zhu, J.; Zhu, H.; Cao, G.; Zhang, J.; Peng, J.; Banjar, H.; Zhang, H.Q. A new mechanistic model to predict boosting pressure of electrical submersible pumps ESPs under high-viscosity fluid flow with validations by experimental data. SPE Gulf Coast Section ESPs Symposium, The Woodlands, USA, May 13-17, 2019a.

158. Zhu, J.; Zhu, H.; Cao, G.; Banjar, H.; Peng, J.; Zhao, Q.; Zhang, H.Q. A new mechanistic model for oil-water emulsion rheology and boosting pressure prediction in electrical submersible pumps ESP. Proceedings of the SPE Annual Technical Conference and Exhibition, Alberta, Canada, Sep 30 – Oct 02, 2019b.

159. Zuber, N.; Findlay, J. Average volumetric concentration in two-phase flow systems. *J. Heat Transfer* **1965**, *87*, pp. 453–468. doi: 10.1115/1.3689137